



Michigan Technological University  
*Create the Future* Digital Commons @ Michigan Tech

---

Dissertations, Master's Theses and Master's  
Reports - Open

Dissertations, Master's Theses and Master's  
Reports

---

2011

## High temperature, low cycle fatigue of a hybrid particulate/fiber aluminum metal-matrix composite

Justin Clark  
*Michigan Technological University*

Follow this and additional works at: <https://digitalcommons.mtu.edu/etds>

 Part of the [Engineering Science and Materials Commons](#)


Copyright 2011 Justin Clark

---

### Recommended Citation

Clark, Justin, "High temperature, low cycle fatigue of a hybrid particulate/fiber aluminum metal-matrix composite ", Master's Thesis, Michigan Technological University, 2011.  
<https://doi.org/10.37099/mtu.dc.etds/26>

Follow this and additional works at: <https://digitalcommons.mtu.edu/etds>

 Part of the [Engineering Science and Materials Commons](#)

HIGH TEMPERATURE, LOW CYCLE FATIGUE OF A HYBRID PARTICULATE/FIBER  
ALUMINUM METAL-MATRIX COMPOSITE

By

Justin Clark

A THESIS

Submitted in partial fulfillment of the requirements for the degree of

MASTER OF SCIENCE

(Materials Science and Engineering)

MICHIGAN TECHNOLOGICAL UNIVERSITY

2011

© Justin Clark 2011

This thesis “High Temperature, Low Cycle Fatigue of a Hybrid  
Particulate/Fiber Aluminum Metal-Matrix Composite,” is hereby approved in  
partial fulfillment of the requirements for the Degree of MASTER OF SCIENCE  
IN MATERIALS SCIENCE AND ENGINEERING.

Department of Materials Science and Engineering

Signatures:

Thesis Advisor: \_\_\_\_\_

Dr. Paul Sanders

Department Chair: \_\_\_\_\_

Dr. Mark Plichta

Date: \_\_\_\_\_

To my parents, who knew that I was not destroying my toys, I was figuring out how they worked.



# Table of Contents

Table of Contents .....	iv
List of Figures .....	vii
List of Tables .....	x
Abstract .....	xi
1. Introduction and Background .....	1
1.1 Metal Matrix Composites.....	1
1.2 Choice of composite .....	1
1.2.1 Property tailoring.....	1
1.2.2 Matrix .....	2
1.2.3 Reinforcement .....	2
1.2.4 Enfil Fiber .....	5
1.2.5 Saffil Fiber .....	6
1.3 Fatigue of MMCs .....	7
1.4 Reactions between reinforcement and matrix .....	8
1.4.1 Silicon Carbide - Matrix.....	8
1.4.2 Alumina - Matrix .....	8
1.4.3 Silica - Matrix.....	9
1.4.4 Effect of interface reaction on mechanical properties .....	9
1.5 Hypothesis.....	9
1.5.1 Shot particle content .....	9
1.5.2 Failure mode.....	9
1.6 MMC Production .....	10
1.7 MMCs in brake drums .....	11
1.8 Modeling .....	13
2. Experimental Procedure .....	15
2.1 Materials.....	15
2.2 Sample Preparation.....	15
2.3 High Temperature Dwell.....	18
2.4 High Temperature Tensile.....	18
2.5 Fatigue .....	18

2.6 Creep .....	20
2.7 Microstructural Examination .....	20
2.7.1 Particle Fracture .....	21
2.8 Temperature Control .....	21
3. Results .....	23
3.1 Dwell Testing .....	23
3.1.1 SiC-Matrix Interface .....	23
3.1.2 Fiber-Matrix Interface .....	24
3.1.3 Matrix Eutectic Si .....	25
3.1.4 Overall effect.....	26
3.2 Elevated Temperature Tensile .....	26
3.2.1 Mechanical properties .....	26
3.2.2 Fracture surface .....	28
3.3 Fatigue .....	30
3.4 Fiber content on fracture surface .....	36
3.5 Microstructure of fatigue samples .....	39
3.5.1 240°C testing .....	39
3.5.2 413°C testing .....	42
3.6 Particle Fracture Progression .....	45
3.7 Origin of dimples on fracture surface .....	47
3.8 Component role in final failure of composite.....	48
3.9 Creep .....	49
4. Discussion.....	53
4.1 Modeling .....	53
4.1.1 Observed particle fracture .....	53
4.1.2 Calculating particle fracture .....	58
4.1.3 Particle Strength Distribution .....	58
4.1.4 Matrix Yielding .....	59
4.1.5 Matrix Recovery .....	59
4.1.6 Composite Creep.....	59
5. Future work .....	64
5.1 Fiber-matrix interface .....	64

5.2Fiber alignment .....	64
5.3Interaction between creep and fatigue .....	64
6. Conclusions .....	65
6.1 Hypothesis.....	65
6.1.1 Shot particle content .....	65
6.1.2 Failure Mode .....	65
6.2Modeling .....	66
7. Works Cited .....	67
Appendix A: Fatigue results .....	70
Appendix B: Stress distribution in fatigue samples.....	72
Appendix C: Tensile Data .....	73
Appendix D: Model Code for observed particle fracture .....	74
Appendix E: Model code for calculated particle fracture .....	77
Appendix F: Additional Matlab functions .....	81
Composite Modulus .....	81
Weibull size distribution .....	81
Work hardening matrix strain.....	81
Ramburg-Osgood matrix strain .....	81
Appendix G: Displacement due to plastic strain from yielding .....	82
Appendix H: T-test for fatigue tests .....	83

## List of Figures

Figure 1.1: Microstructure of Enfil fiber MMC .....	6
Figure 1.2: Microstructure of Saffil fiber MMC .....	7
Figure 1.3: Schematic of preform infiltration by squeeze casting.....	11
Figure 2.1: Century Inc. Al MMC brake drum with selectively reinforced wear surface .....	16
Figure 2.2: Fiber orientation in brake drum wear surface as viewed from the open end of the drum .....	16
Figure 2.3: Saffil fiber samples sectioned perpendicular to the open end of the drum and parallel to the axis of the drum (a) and at parallel to the open end and perpendicular to the axis of the drum (b) .....	17
Figure 2.4: Fatigue bar dimensions (in) .....	17
Figure 2.5: Tensile Bar Dimensions (in) .....	18
Figure 2.6: Thermocouple locations for temperature distribution measurement (in) .....	21
Figure 2.7: Temperature profile of fatigue samples during induction heater on servo-hydraulic test frame used in this study.....	22
Figure 3.1: Optical metallography of Saffil samples before (a) and after (b) dwell testing at 240°C for 100hr. ....	23
Figure 3.2: Optical metallography of Enfil samples before (a) and after (b) dwell testing at 240°C for 100hr. ....	24
Figure 3.3: Back Scattered Electron images of Enfil fiber MMCs before (a) and after (b) dwell testing at 240°C for 100hr.....	25
Figure 3.4: Eutectic Si structure before (a) and after (b) dwell at 240°C for 100hr. ....	26
Figure 3.5: Stress-Strain Curves for Enfil and Saffil MMCs and Monolithic A356 at 240°C .....	27
Figure 3.6: Fracture surface of Saffil (a) and Enfil (b) tensile samples tested at 240°C.....	28

Figure 3.7: High magnification fracture tensile fracture surfaces of Saffil (a) and Enfil (b) tested at 240°C .....	29
Figure 3.8: 240°C Fatigue Results for Enfil and Saffil MMCs.....	31
Figure 3.9: 413°C Fatigue Results for Enfil and Saffil MMCs.....	31
Figure 3.10: Fracture Surfaces of Saffil (a) (maximum stress 140Mpa) and Enfil (b) (Maximum stress 120MPa) fiber fatigue samples tested at 240°C ...	32
Figure 3.11: High magnification images of Saffil (top) and Enfil (bottom) fiber samples tested in fatigue at 240°C with a maximum stress of 120MPa ..	33
Figure 3.12: Fatigue sample failed on plane ~45° to loading direction .....	34
Figure 3.13: Influence of fiber orientation on plane of failure .....	34
Figure 3.14: Microstructure of fatigue sample viewed in plane a (a) and in plane b (b) from Figure 3.13 showing fiber orientation. ....	35
Figure 3.15: Hackle marks on a SiC particle in a Saffil sample tested in fatigue at 240°C indicating brittle failure of the particle .....	36
Figure 3.16: Fiber and shot on fracture surface of Enfil fiber MMC .....	37
Figure 3.17: Fiber content on creep fracture surface of Saffil (a) and Enfil (b) fiber MMCs tested at 240°C at a stress of 68.9MPa .....	38
Figure 3.18: Microstructure of Saffil samples after fatigue testing at 240°C. ....	40
Figure 3.19: Microstructure of Enfil samples after fatigue testing at 240°C. ....	41
Figure 3.20: Saffil samples after fatigue testing at 413°C. Fewer SiC particles have broken than in samples tested at 240°C.....	43
Figure 3.21: Enfil fiber samples after fatigue testing at 413°C. Fewer SiC particles have broken than in samples tested at 240°C .....	44
Figure 3.22: Microstructure of MMCs tested for 0 (a), 10,000 (b), 100,000 (c), and 1,000,000 (d) cycles.....	46
Figure 3.23: Particle fracture progression for samples tested at 240°C with a max stress of 100MPa.....	46
Figure 3.24: Fractured SiC particle and dimples in the matrix .....	48
Figure 3.25: 82.7MPa creep (a) and 120MPa fatigue (b) fracture surfaces tested at 240°C .....	51

Figure 3.26: Microstructure of Saffil (a) and Enfil (b) samples after 68.9MPa creep testing at 240°C .....	52
Figure 4.1: Procedure for calculating composite stress strain curve .....	56
Figure 4.2: Maximum stress in matrix and SiC particles and matrix UTS as calculated by the model .....	58
Figure 4.3: Average cross-head displacement and stroke for fatigue test with maximum stress of 100MPa at 240°C .....	60
Figure 4.4: Method used to calculate fatigue behavior of composite based on calculated particle fracture .....	61
Figure 4.5: Calculated and observed SiC particle volume fraction for testing at 465°F with a maximum stress of 100MPa .....	62
Figure 4.6: Maximum stress in matrix and SiC particles and matrix UTS based on calculated particle volume fraction .....	63
Figure B.1: radius of sample as a function of distance from center .....	72
Figure B.2: Stress in sample as a function of distance from center .....	72
Figure G.1: Schematic composite stress-strain curve.....	82
Figure H.1: T-test results for fatigue at 240°C with a maximum stress of 140MPa .....	83
Figure H.2: T-test results for fatigue at 240°C with a maximum stress of 120MPa .....	83
Figure H.3:T-test results for fatigue at 240°C with a maximum stress of 100MPa .....	84
Figure H.4:T-test results for fatigue at 413°C with a maximum stress of 140MPa .....	84
Figure H.5:T-test results for fatigue at 413°C with a maximum stress of 120MPa .....	85
Figure H.6:T-test results for fatigue at 413°C with a maximum stress of 100MPa .....	85

## List of Tables

Table 1.1: Chemical composition of A356 matrix .....	2
Table 1.2: Properties of SiC at room temperature .....	3
Table 1.3: Chemical composition and shot content of Saffil and Enfil fibers ...	6
Table 1.4: Thermal properties of monolithic A357, A357 MMC, and Cast Iron .	12
Table 1.5: Room temperature tensile properties of hybrid MMC and monolithic A356 from the current study .....	13
Table 2.1: Temperature-Load combinations to be tested in fatigue .....	19
Table 2.2: Testing Conditions in terms of service conditions of brake drum ...	19
Table 3.1: Tensile Properties of Enfil MMC, Saffil MMC, and monolithic A356 at 240° C.....	27
Table 3.2: Composite component role in final fatigue failure .....	49
Table 3.3: Creep Results at 240° C .....	50
Table 4.1: Experimental and rule of mixtures elastic modulus for Saffil fiber MMC at room temperature .....	54
Table 4.2: Ultimate Tensile strength of A356 as a function of time at 240° C .	57
Table A.1: Fatigue results for all samples tested.....	71
Table C.1: Tensile results for all samples tested .....	73

## **Acknowledgements**

I would like to thank Century Inc. (Traverse City, MI) for supplying brake drums for samples. Special thanks also to GS Engineering Inc. (Houghton, MI) for sharing their knowledge and invaluable discussions.

I would also like to thank my fellow students who helped me through my course work and research. They provided me a resource to help me work through problems that inevitably came up.



## **Abstract**

The effect of shot particles on the high temperature, low cycle fatigue of a hybrid fiber/particulate metal-matrix composite (MMC) was studied. Two hybrid composites with the general composition A356/35%SiC particle/5%Fiber (one without shot) were tested.

It was found that shot particles acting as stress concentrators had little effect on the fatigue performance. It appears that fibers with a high silica content were more likely to debond from the matrix.

Final failure of the composite was found to occur preferentially in the matrix. SiC particles fracture progressively during fatigue testing, leading to higher stress in the matrix, and final failure by matrix overload.

A continuum mechanics based model was developed to predict failure in fatigue based on the tensile properties of the matrix and particles. By accounting for matrix yielding and recovery, composite creep and particle strength distribution, failure of the composite was predicted.

# 1. Introduction and Background

## 1.1 Metal Matrix Composites

Metal Matrix Composites (MMCs) typically consist of a ductile metal matrix (Al, Mg, Cu, Ti, etc.) and a high modulus ceramic reinforcement (SiC, Al<sub>2</sub>O<sub>3</sub>, TiC, etc.) The combination of multiple materials results in a material that can have the advantageous properties of both components. The matrix provides ductility and high thermal and electrical conductivity. The high modulus ceramic reinforcement acts to strengthen the material and makes the composite stiffer; it can also act to restrict the thermal expansion of the composite. The mechanism of the composite strengthening from the reinforcement phase is dependent on shape, size, and volume fraction. Small particles can act to strengthen the composite through Orowan dispersion mechanisms. Large particles do not impart much Orowan strengthening (Nan and Clarke 1995). In MMCs with large particles, the composite is strengthened by load transfer from the matrix to the particle where the particles carry a significant portion of the load.

MMCs can also be reinforced with short fibers. These fibers act to strengthen the composite in a manner similar to large particle reinforced composites. Load is transferred to the fibers along the fiber-matrix interface. The high aspect ratio of fibers results in greater strengthening along the fiber's long axis.

With the use of MMCs it is possible to achieve properties that would not be obtainable with any of the constituent materials alone. For example, it is possible to create a material with high thermal conductivity that has a low thermal expansion. With the correct reinforcement selection, it is also possible to increase the wear resistance of a soft metal such as Al or Mg.

## 1.2 Choice of composite

### 1.2.1 Property tailoring

The desired properties of the composite determine what matrix, reinforcing phase(s), and reinforcement volume fraction are used. High strengths can be achieved by using a large reinforcing phase volume fraction. As is often the case, there is a trade off resulting in low ductility when achieving high strengths.

### 1.2.2 Matrix

The choice of matrix material can depend on reinforcement phase composition. Chemical reactions can occur at the interface between matrix and reinforcement. Some of these reactions will be discussed in section 1.4.

Processing route for manufacturing of the component also influences choice of matrix metal. Alloys that work well for powder processed MMCs might not work well for cast MMCs.

In the current study, the matrix of the MMC was a Sr modified A356. This alloy was chosen as it is a common casting alloy and it has a Si level that should act to limit chemical reaction with the reinforcement. The composition of A356 can be found in Table 1.1.

At temperatures over 200°C monolithic A356 fracture surfaces show microscopic cup and cone type failure indicative of ductile failure (Brosnan and Shivkumar 1995). At a temperature of 250°C Brosnan and Shivkumar observed that permanent mold cast A356 showed a high degree of necking, leading formation of voids in the matrix.

*Table 1.1*

*Chemical composition of A356 matrix  
(Aluminum Association Record 99)*

Element	Wt %
Al	91.1 - 93.2 %
Si	6.50 - 7.50 %
Mg	0.30 - 0.45 %
Cu	<= 0.20 %
Fe	<= 0.15 %
Mn	<= 0.10 %
Ti	<= 0.20 %
Zn	<= 0.10 %
Other, each	<= 0.050 %
Other, total	<= 0.15 %

### 1.2.3 Reinforcement

By choosing the reinforcement phase size, morphology, and volume fraction, it is possible to tailor the properties of the composite to fit a desired application.

Small ( $<10\mu\text{m}$ ) particles will lead to dispersion/Orowan strengthening by acting as barriers to dislocation movement (He 2011). Particles of this size act to strengthen the matrix in a manner similar to precipitates in an age hardenable alloy.

If a wear resistant material is desired, large ( $>15\mu\text{m}$ ) particles have been shown to increase both the strength and wear resistance of composite over the monolithic metal (Lloyd 1994). These large particles do not impart as much strength to the composite as smaller particles. The spacing of large particles is too great for significant Orowan strengthening. The main strengthening mechanism for composites with large particles is load transfer to the particles from the matrix. Through this load transfer, particles carry the majority of the load in a composite. Some of the material properties of SiC can be found in Table 1.2.

*Table 1.2*  
*Properties of SiC at room temperature*  
*(Snead, et al. 2007)*

Elastic Modulus (GPa)	415
Ultimate Tensile Strength (MPa)	250
Weibull Modulus	3-11

Previous researchers have found that tensile failure in particulate reinforced composites is often a result of either particle fracture or debonding from the matrix (Babout, et al. 2004). Which failure mechanism is dominant for a given system is dependent on the strength of the interface between particle and the matrix.

Large particles have been found to fracture preferentially in particulate reinforced MMCs (Zong and Derby 1993). Large particles have a lower fracture stress as described by the Griffith fracture criterion.

High strength can also be achieved through the addition of ceramics in the form of fibers (Ochi 2007). Fibers are often short (hundreds of microns) and can be aligned, random-planar, or randomly oriented. Fibers act to strengthen the composite by carrying a large portion of the load placed on the composite. They introduce anisotropy to the composite as load is transferred

to fibers by shear stress from the matrix along the length of the fiber parallel to the loading direction. If a fiber is oriented transversely to the loading direction, the distance over which the fiber is able to be loaded is not great enough to reach the fiber fracture strength leading to less strengthening.

Randomly aligned fibers give the material isotropic properties. Random-planar aligned fibers give isotropic properties in directions parallel to the plane in which fibers lay. Most composites with aligned short fibers have a random-planar alignment where fibers are randomly oriented in a single plane (Rafiquzzaman 2008). While isotropy is desirable in some applications, there are applications where strength in a single direction is more important, such as a brake drum. The majority of stress in a brake drum is in the hoop direction. Therefore aligning fibers in the hoop direction will give the best properties for the application. For applications where strength in a single direction is desirable, aligned short fiber composites are a good solution; however, aligning short fibers in a single direction is difficult. Few manufacturing methods are able to align the majority of fibers in a single direction. Often fibers are either completely randomly oriented or randomly oriented on a single plane. While continuously reinforced fiber MMCs exist, they will not be discussed in this work.

MMC's are often classified by the morphology of the reinforcement; the most common forms of which are fibers and particles. In most cases, only one reinforcement morphology is used. However there are situations in which utilizing multiple reinforcement types is advantageous. Composites with multiple reinforcement morphologies are known as hybrid composites. Their study has been extremely limited (Rafiquzzaman 2008). To date, most work on hybrid composites has been done at room temperature. However, many of the possible applications of MMCs will encounter high temperature during service.

In hybrid composites, the choice of fiber is important to the strength of the final MMC. It has been shown that failure in hybrid composites initiates at defects such as clusters of fibers and shot particles (Rafiquzzaman 2008). Shot particles will be discussed in section 1.2.4. The failure mode is also dependent on the interface between fiber and matrix. If the interface between fiber and matrix is weak, the fiber will likely de-bond from the matrix. It can then pull away from the matrix with little work. If the interface between fiber and matrix is strong the fiber will likely fracture rather than de-bond. The fracture of a fiber takes a significant amount of energy resulting in a stronger composite.

Fibers can vary in composition and aspect ratio. The proper choice of fiber is dependent on the desired properties of the composite as well as cost. Two possible fiber choices for an MMC in this study are an aluminosilicate fiber (Enfil) and a high purity alumina (Saffil) fiber. These fibers differ in both composition and presence of shot particles. The aspect ratio of the fibers used in this study was the same.

#### **1.2.4 Enfil Fiber**

Enfil fiber is an aluminosilicate fiber, consisting of a mixture of alumina and silica. The fiber is manufactured using a high pressure air attenuation process that forms defects known as shot particles. These particles form as liquid droplets on the end of a fiber that solidify as the molten fiber cools. Shot particles are large, circular or teardrop shaped, and often hollow. A representative microstructure of an Enfil fiber hybrid MMC including shot particles is shown in Figure 1.1. These shot particles can be fractured in the fiber manufacturing process and therefore have significantly reduced mechanical properties compared to the fiber. They can also act as stress concentrators. Broken particles have sharp It has been shown that fatigue cracks can initiate on these particles in fiber reinforced MMCs (Herr et al. 1995); (Lesuer 1998). Since shot particles are the largest microstructural feature, they can contain the largest defects making them the easiest feature for a crack to initiate on. Lesuer found the fatigue strength of an Al MMC decreased as the size of shot particles increased (Lesuer 1998).

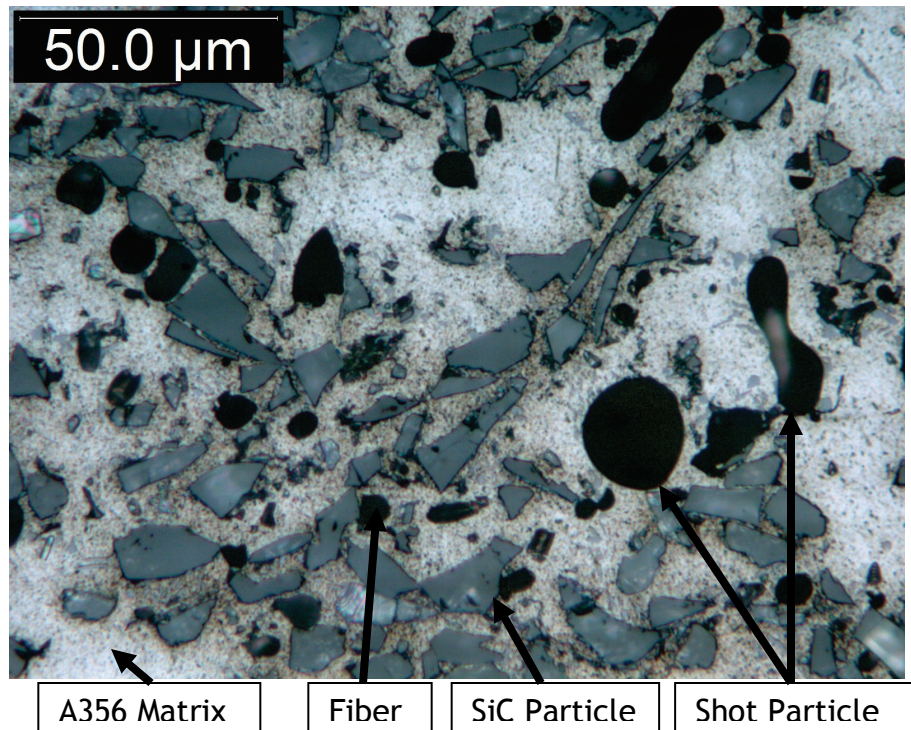


*Figure 1.1: Microstructure of A356/35%SiC particle/5% Enfil fiber MMC showing presence and size of shot particles.*

*(fibers are viewed end on)*

#### 1.2.5 Saffil Fiber

Saffil fiber is a high purity alumina fiber that is manufactured by a chemical process that results in a fiber that is effectively shot free. This process is 5 times more expensive than the process used to manufacture Enfil fiber. Typical fiber compositions and shot contents of both Saffil and Enfil fibers are shown Table 1.3. Figure 1.2 shows a representative microstructure of a Saffil fiber hybrid MMC. Little work has been done to examine the effect of shot particles on hybrid reinforced MMCs.

*Table 1.3*

*Chemical composition and shot content of Saffil and Enfil fibers*

*(From fiber supplier)*

	Weight %	
	Saffil	Enfil
Alumina	96	46
Silica	4	54
Shot Content	0	4.5

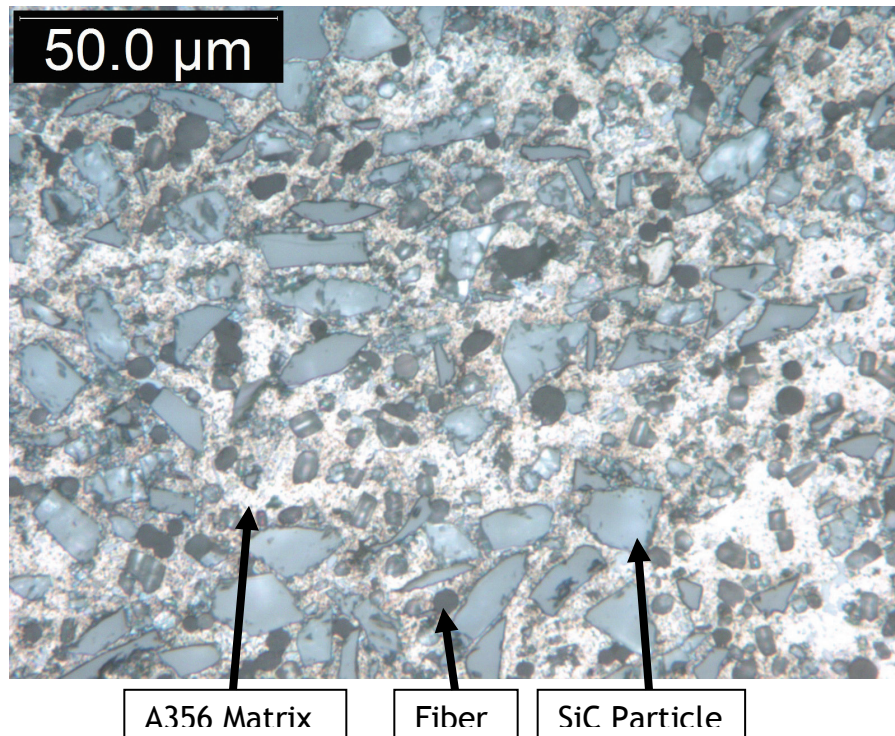


*Figure 1.2: Microstructure of an A356/35%SiC particle/5%Saffil fiber MMC showing a lack of large shot particles.*

*(fibers are viewed end on)*

### 1.3 Fatigue of MMCs

Generally, fatigue performance of a material is dependent on the ease of crack initiation and growth. For many systems, the addition of SiC particles has been found to increase the fatigue performance over the monolithic matrix metal (Hall et al. 1994). Additions of alumina fibers can improve the fatigue performance of both Al and Mg (Ochi 2007).

Others have found that the classic fatigue features of crack initiation, growth, and final failure are present on the fracture surface of both particle and short fiber reinforced MMCs (Herr et al. 1995; Srivatsan 2002a). A crack initiation site can be a region of a sample with reduced mechanical properties. Material defects such as porosity can also act as crack initiation sites. Cracks often initiate at shot particles or short fibers in fiber reinforced MMCs (Ding 2002; Ochi 2007). In particulate reinforced composites, cracks initiation occurred at clusters of particles (Srivatsan 2002a). Since the composite investigated in this study contains both fibers and particles, both types initiation sites for failure initiation are possible. Previous room temperature

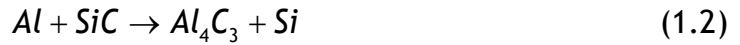


studies found that fatigue damage initiation occurs both at clusters of fibers and shot particles in hybrid MMCs (Rafiquzzaman 2008).

## 1.4 Reactions between reinforcement and matrix

### 1.4.1 Silicon Carbide - Matrix

The interface between reinforcement and matrix is a concern in MMCs. The interface is responsible for transferring load between matrix and reinforcement. Interface reactions have been observed in Al/SiC composites manufactured using a liquid phase process (Evans 2003). Multiple reaction products have been suggested as shown in equations 1.1 and 1.2.



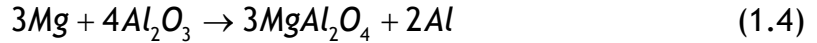
Reactions 1.1 and 1.2 only occur when SiC particles are in contact with liquid aluminum as SiC is stable below the solidus. Sritharan reported that an interface reaction between SiC particles and Al will leave pits and ledges on the SiC particles that are visible by optical metallography (Sritharan 2001).

Reactions 1.1 and 1.2 can be limited by using a matrix metal that is high in silicon to reduce the driving force for the reaction. The A356 matrix used in the composites in this study has a Si content of 7% which should limit the reactivity of SiC in molten Al. The squeeze casting process used in this study also limited the time in which SiC particles were exposed to liquid Al. Both of these factors acted to limit interface reactions between particles and matrix during the manufacturing of the MMCs in this study. Examination of the as received microstructures, as seen in Figure 1.1 and Figure 1.2, shows no evidence of pits and ledges. This shows that little if any interface reaction has occurred during casting.

### 1.4.2 Alumina - Matrix

Alumina is stable in pure aluminum but can react with magnesium present in the matrix to form the reaction products shown in equations 1.3 and 1.4 (Lloyd 1994). The A356 matrix in the present study has a Mg content of 0.3% so reactions between the matrix and the alumina in both fibers is possible.

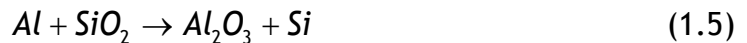




Unlike the SiC in Al, alumina is not stable below the solidus, so reactions can occur or continue in the solid state. The reaction between alumina and the matrix in solid state could become important when exposure to high temperatures for long times is expected in service.

#### 1.4.3 Silica - Matrix

A reaction between silica present in Enfil fiber and a binder used in both MMCs could also proceed according to equation 1.5.



Since Enfil fiber is an aluminosilicate, the silica in the fiber has the potential to react with the matrix unlike Saffil fiber which is pure alumina. Like the reaction between alumina and Al, reaction between silica and Al is possible in the solid state.

#### 1.4.4 Effect of interface reaction on mechanical properties

Interface reactions have been found to be detrimental to mechanical properties of MMCs reducing their ductility (Tham et al. 2003). They can also influence the failure mode of a composite. Evans (2003) reported that failure in tension was a result of failure in a 40nm thick amorphous layer containing Si, Mg, Al, and O that formed between SiC particles and a 2080 matrix. (3.6% Mg, 0.25% Cu, 0.25% Zr) It was found that decohesion of particles and the matrix proceeded through this layer.

### 1.5 Hypothesis

#### 1.5.1 Shot particle content

The reduced shot content of Saffil fiber compared to Enfil fiber will result in higher cycles to failure in fatigue. Shot particles are the largest microstructural feature and therefore can contain the largest flaws. Cracks will initiate from these flaws leading to failure. Fewer shot particles will give fewer “defects” in the material from which cracks are able to initiate and grow.

#### 1.5.2 Failure mode

SiC particle fracture during fatigue testing will lead to overloading of the matrix being the dominant failure mechanism. Once a particle is broken, its ability to carry load effectively becomes zero. For the composite to carry the same load, the matrix experiences a greater stress. Final failure of the MMC

will occur when the stress in the matrix exceeds the UTS of the monolithic matrix material.

### **1.6 MMC Production**

There are multiple processing routes for manufacturing MMCs, including powder processing, stir casting, and preform infiltration. Samples in this study were made utilizing a squeeze casting preform infiltration process. This process allows for selective reinforcement only in the areas where the performance of an MMC is needed. The rest of the part can be a monolithic matrix material which retains the properties of the matrix metal such as high ductility. The monolithic matrix material can also be machined with standard tooling unlike the MMC which requires diamond tooling.

In the preform infiltration manufacturing method, the ceramic component of the MMC is formed into a ceramic sponge called a preform. The ceramic is mixed with a silica binder, organic fillers, and water. It is then formed into the desired shape and dried. Once dry, the green preform undergoes thermal processing to burn out the fillers and set the binder. The spaces once occupied by organics become porosity in the preform. By controlling the porosity of this preform, the volume fraction of reinforcement in the final MMC can be controlled. The finished preform can then be infiltrated with molten metal to create an MMC. Pressure has to be applied to the molten metal in order for complete infiltration to occur. This pressure is applied by squeeze casting Al into and around the preform (Figure 1.3).

Homogeneity is an important consideration in composites. It has been shown that cracks can initiate at clusters of particles or fibers in MMCs (Ochi 2007; He 2011). Other manufacturing methods such as stir casting, lead to clustering of particles as they are pushed to the interdendritic regions during solidification. The preform infiltration process helps to eliminate this problem by fixing the position of the ceramic components during casting.

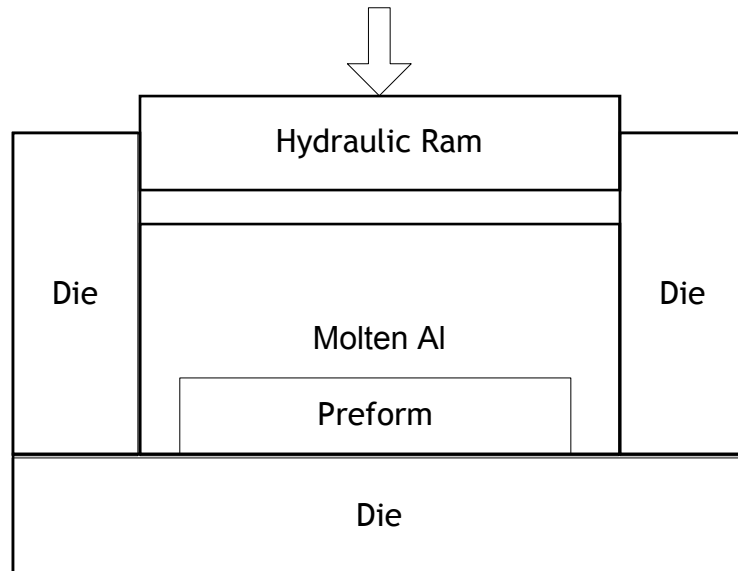


*Figure 1.3: Schematic of preform infiltration by squeeze casting. Molten Al is forced into the preform by the application of hydraulic pressure to create the composite.*

*Adapted from (Dieringa et al. 2004)*

Conventionally, preforms are produced using a batch vacuum slurry forming process. This can lead to poor mixing of the components and defects such as clusters of fibers. The slurry process also leads to a planar alignment of fibers. Preforms in this study were manufactured using a twelve screw extruder from Century Inc. (Traverse City, Michigan) that homogeneously mixes the SiC particles and ceramic fibers with the organics and binder. Extruding the preform material with the twelve screw design breaks up fiber clumps and distributes the fibers throughout the preform. It also acts to align fibers in a single direction resulting in an aligned short fiber hybrid MMC.

### **1.7 MMCs in brake drums**

To be successful, any materials used in brake drums need to have desirable tensile and fatigue properties at elevated temperatures. Currently, most heavy duty trucks utilize cast iron brake drums. Aluminum MMCs are a potential replacement material with significantly reduced weight without loss of performance. The incorporation of large ceramic particles can increase the wear resistance of Al making it possible to manufacture a brake drum with very long life before needing to be replaced due to wear. The long wear life makes the fatigue properties of an MMC of great interest. A wear surface that will last for a million miles will not be useful if the drum fails from fatigue after 1000 miles.

Brake systems convert the kinetic energy of a moving vehicle to heat by applying friction to the braking surface. Temperatures of up to 296 °C (565 °F) are commonly observed in dynamometer testing of cast iron drums. While an Al MMC drum has to convert the same amount of kinetic energy to heat it does not heat up as much as cast iron. Performing the same test on a MMC drum resulted in temperatures of 227 °C (440 °F). The reduction in temperature is due to the thermal properties of Al. Al has a higher thermal capacity than cast iron; it can absorb almost twice as much energy per unit volume compared to iron without heating up. Al also has a higher thermal diffusivity (thermal conductivity divided by the product of the heat capacity and density) giving it the ability to shed heat away from the friction surface and into the bulk of the drum faster. While the addition of reinforcing particles (SiC, Al<sub>2</sub>O<sub>3</sub>) does reduce the thermal capacity and thermal conductivity of Al, the effect is small. The thermal data for A357 (similar to the A356 used in this study), an A357 MMC of the same composite composition studied in this work, and Cast Iron can be found in Table 1.4. Finite Element Analysis (FEA) simulation of the FMVSS 121 vehicle test has shown temperatures of 452 °C (845 °F) may be possible on the friction surface of an Al MMC drum under extreme braking events. All FEA calculations were conducted by GS Engineering, Houghton, MI.

*Table 1.4*

*Thermal properties of monolithic A357, A357 MMC, and Cast Iron  
(MMC data courtesy of GS Engineering, Houghton, MI)*

	Heat Capacity at 20 °C $\left( \frac{J}{kg \cdot K} \right)$	Thermal Expansion Coefficient ( $\times 10^{-6} / ^\circ C$ )	Thermal Diffusivity at 23 °C $\left( \frac{m^2}{s} \right)$ $\times 10^{-5}$
A357	880	21.6	6.219
A357 MMC	798	12.2	4.544
Cast Iron (ASTM 40)	490	9	1.51

Room temperature tensile properties of both Saffil and Enfil MMCs used in this study have been studied extensively. Table 1.5 shows typical room temperature properties of both Saffil and Enfil MMCs. However, the elevated temperature properties have not been studied in depth before this study.

Table 1.5

*Room temperature tensile properties of hybrid MMC and monolithic A356 from the current study*

	Saffil+SiC MMC T5	Enfil+SiC MMC T5	A356 T5
Modulus (GPa)	131	145	69
$\sigma^{UTS}$ (MPa)	269	255	228
$\sigma^Y$ (MPa)	186	172	144
Strain at failure (%)	0.52	0.43	5.2

### 1.8 Modeling

Multiple methods for calculating the mechanical behavior of MMCs have been developed. The choice of which method best predicts behavior is dependent on the composite being examined. Models that incorporate the strengthening from dispersion effects of the reinforcement particles can predict the properties of composites with small ( $<1\mu\text{m}$ ) particles. The small reinforcing particles act as barriers to dislocation motion. Dislocations have to bow around the particle in order to pass through the matrix. Reinforcing particles act to strengthen the composite in similar to how a precipitate in an age hardenable alloy strengthens the alloy. Models based on treating reinforcement particles as dispersion hardening phases begins to fall apart as the volume fraction and particle size of reinforcement particles increases. As the size of the particles become large, the center to center spacing between particles becomes too large for dispersion strengthening to be significant. For the composites in this study, the spacing between SiC particles was approximately  $50\mu\text{m}$ .

Other researchers have utilized Finite Element Analysis (FEA) to model the stress field in and around particles in MMCs (Wang et al. 1993); (Watt et al. 1996). Results have shown that the stress in the matrix near the particle interface to be significantly higher than the average stress in the composite. These FEA models are useful when looking at consistent distributions of uniformly shaped and sized reinforcement components. While the structure of continuously reinforced composites lend themselves to this type of analysis, the nature of discontinuously reinforced MMCs makes FEA analysis difficult. The random distribution and size variation of particles make it difficult to

examine the stress distribution in a composite without having a microstructure to start with.

In composites where the reinforcement particles are larger than  $10\mu\text{m}$ , a continuum approach yields better results in describing the mechanical behavior of composites. Eshelby developed a series of thought experiments for examining the stresses experienced in a system consisting of a strong, stiff particle embedded in a ductile matrix (Eshelby 1957; Eshelby 1959). Eshelby's model assumed an ellipsoidal particle, others have examined other particle geometries (Brown 1975). While this approach was derived for the examination of precipitation hardened materials, it can be applied to metal matrix composites.

An effective medium approach based on an Eshelby approach of examining the stresses in both the matrix and particle was used in the current work. Corbin and Wilkinson developed a model that allows for the prediction of tensile behavior of a composite knowing only the stress-strain behavior of the matrix and particles, and the volume fraction of particles (S.F. Corbin 1993). Their model treats the composite as a network of two phases (the matrix and reinforcing particles) in an effective medium. This model assumes that there is no damage to the particles during testing. This assumption leads to poor results at high strain values. Others include a Griffith fracture criterion to SiC particles to account for particle fracture observed at high strain (Nan and Clarke 1995). They assumed that particles would fracture based on their size where large particles will fracture at lower stress than smaller ones. The inclusion of particle fracture yields more accurate results at higher strain values.

These models only look at the tensile behavior of the composite. In this study these models are expanded to look at the fatigue behavior of a composite. The approach used to extend these models will be introduced in section 4.1.

## 2. Experimental Procedure

### 2.1 Materials

To study the effect of shot particles on the fatigue and creep performance of a hybrid MMC, two different MMCs of the composition: A356/35%SiC<sub>p</sub>/5%Ceramic<sub>f</sub> were examined. Where the percent is the volume fraction of the component, and the subscript p or f designates the reinforcement morphology (particle or fiber). The two composites differed only in type of ceramic fiber used, samples of both Enfil and Saffil fiber were tested. Saffil fiber samples were free of shot particles, while Enfil fiber samples contained approximately 4.5% by volume shot particles. Both fiber types were approximately 100μm in length and 10μm in diameter. SiC particles were faceted particles with an average diameter 35μm.

### 2.2 Sample Preparation

Samples were machined from the Century 15x4, 15 inch inner diameter with a 4 inch wear surface, lightweight MMC brake drum manufactured by Century Inc. (Traverse City, MI) shown in Figure 2.1. Fiber orientation during the preform manufacturing process aligns fibers in the hoop direction of brake drum as seen in Figure 2.2.

Micrographs both parallel and perpendicular to the open end of the drum show that fibers are seen end on when looking at a cross section that is perpendicular to the open end of the drum and parallel to the drum axis. (Figure 2.3a) Fibers are seen along their length when looked at parallel to the open end and perpendicular to the axis the drum. (Figure 2.3b)

Sample blanks were cut parallel to the axis, Figure 2.1, of the drum resulting in transversely aligned fibers. The fiber orientation in the brake drum made obtaining samples with fibers aligned in the loading direction of the sample impossible. Blanks were cut from the wear surface of the brake drum. All samples were then T5 heat treated at 350°F for 6 hours and water quenched. Fatigue samples were then turned with diamond tooling to ASTM E 466 as seen in Figure 2.4.

All transverse machining marks were removed by hand polishing with metallurgical paper. Progressively finer grits: 240, 320, 400, and 600 grit SiC were used to achieve the final surface finish. Samples were observed under a stereoscope to ensure no transverse marks were visible to validate the polishing procedure. Creep and tensile samples were machined to standard



tensile bar dimensions as seen in Figure 2.5. Tensile and creep samples were tested in the as machined condition.

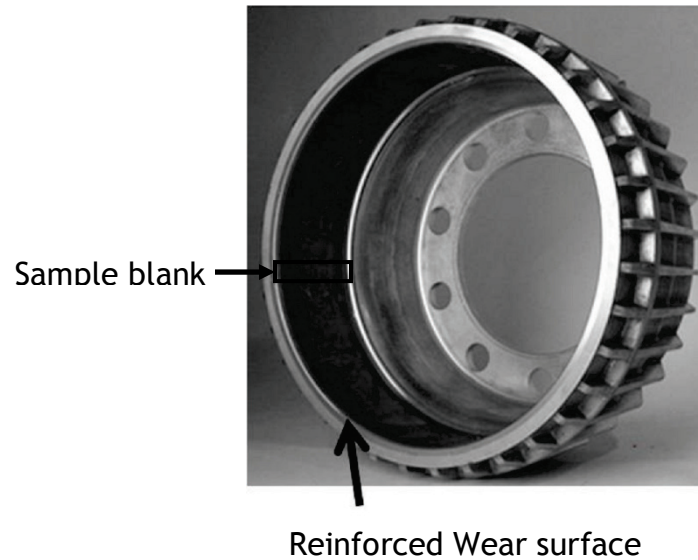


*Figure 2.1: Century Inc. Al MMC brake drum with selectively reinforced wear surface showing orientation of sample blanks.*

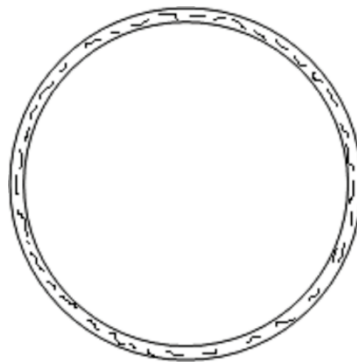


*Figure 2.2: Fiber orientation in brake drum wear surface as viewed from the open end of the drum showing fibers aligned in the hoop direction of the drum.*

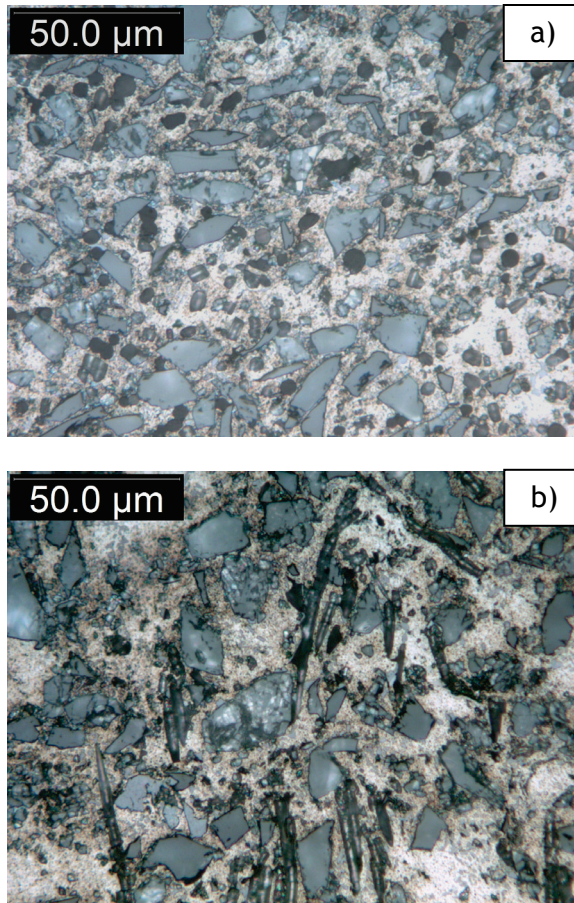


Figure 2.3: Saffil fiber samples sectioned perpendicular to the open end of the drum and parallel to the axis of the drum (a) and at parallel to the open end and perpendicular to the axis of the drum (b) showing fiber orientation.

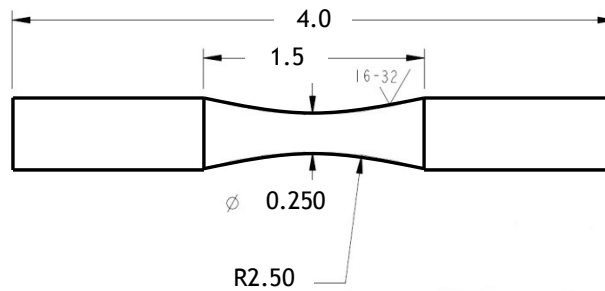
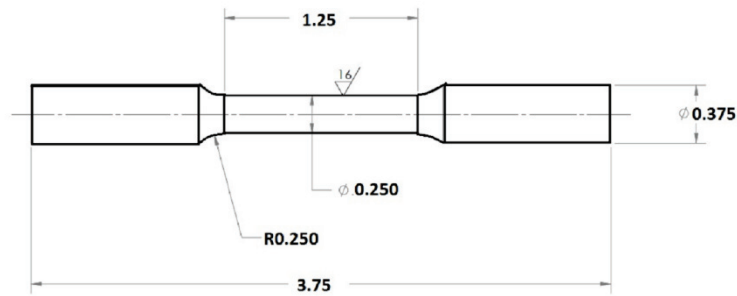


Figure 2.4: Fatigue bar dimensions (in) used in the current study



*Figure 2.5: Tensile Bar Dimensions (in) used in the current study*

### **2.3 High Temperature Dwell**

To determine if interface reactions occur between the reinforcing phases and the matrix during long term exposure to high temperature, dwell testing was conducted. Samples of both Enfil and Saffil fiber MMCs were held at 240°C in a box furnace for 100 hr. This time simulated the average time a fatigue test would run. No mechanical force was applied to the samples to allow for examination of an undamaged structure and to eliminate stress as a variable. Microstructures were observed before and after heating.

### **2.4 High Temperature Tensile**

Samples of Enfil and Saffil fiber MMCs as well as monolithic A356 were tested at 240±5°C to determine mechanical properties. Testing was done in a servo-hydraulic test frame equipped with water cooled hydraulic grips. Samples were inductively heated and tested immediately after test temperature was reached and remained steady. This condition was achieved after approximately one minute of heating. A high temperature extensometer with alumina knives was used to measure strain. The modulus of the material was calculated by finding the slope of the near linear region of the stress-strain curve. Yield stress for all materials was calculated using the offset method.

### **2.5 Fatigue**

Samples were tested at three different temperatures and maximum stress levels. All tests were conducted with an R value of 0.38 and a testing frequency of 20Hz. The R value determines the ratio between maximum and minimum stress. Fatigue tests were carried out at room temperature, 240°C, and 413°F. The eutectic of the A356 matrix used in this study is 557°F resulting in testing at 45% and 75% of the eutectic temperature respectively. Test conditions are shown in Table 2.1. Stress controlled testing was conducted to best simulate conditions observed in service. Test conditions

were selected in order to simulate conditions observed by a brake drum during service (Table 2.2).

The yield stress at 240°F of both MMCs was under 100MPa. This puts all conditions tested at elevated temperatures in the low cycle fatigue regime where plastic deformation can occur during every cycle.

Table 2.1

Temperature-Load combinations to be tested in fatigue

All tests carried out a frequency of 20Hz

Temperature °C (°F)	Load Conditions		
	High Stress MPa (ksi)	Medium Stress MPa (ksi)	Low Stress MPa (ksi)
22 (72)	140±1.38 (20.3 ±0.2)	120±1.03 (17.4 ±0.15)	100±1.03 (14.5 ±0.15)
240±5 (465 ±10)	140±1.38 (20.3 ±0.2)	120±1.03 (17.4 ±0.15)	100±1.03 (14.5 ±0.15)
413±5 (775 ±10)	140±1.38 (20.3 ±0.2)	120±1.03 (17.4 ±0.15)	100±1.03 (14.5 ±0.15)

Table 2.2

Testing Conditions in terms of service conditions of brake drum

	140MPa	120MPa	100MPa
240C	<ul style="list-style-type: none"> <li>• Very hard braking</li> <li>• Average service temperature</li> </ul>	<ul style="list-style-type: none"> <li>• Hard braking</li> <li>• Average service temperature</li> </ul>	<ul style="list-style-type: none"> <li>• Average braking</li> <li>• Average service temperature</li> </ul>
413C	<ul style="list-style-type: none"> <li>• Very hard braking</li> <li>• Well above average service temperature</li> </ul>	<ul style="list-style-type: none"> <li>• Hard braking</li> <li>• Well above average service temperature</li> </ul>	<ul style="list-style-type: none"> <li>• Average braking</li> <li>• Well above average service temperature</li> </ul>

Tests were performed on a servo hydraulic test frame that was aligned to minimize any bending stresses. Test samples were held in water cooled, hydraulically actuated wedge grips. Samples were inductively heated to the test temperature and controlled to ±5°C. Testing began immediately upon

reaching test temperature with no hold at temperature. This condition was achieved after approximately one minute of heating.

Tests were carried out until failure by fracture or run out. Run out was defined as 11.5 million cycles. This number of cycles would be representative of approximately 10,000 miles of heavy braking events on a vehicle. Assuming approximately 2% of the vehicle duty cycle is braking events, 10,000 miles of braking events translates into 500,000 vehicle miles.

Hydraulic actuator position as well as load data was collected as a function of cycle to examine both composite yielding and creep behavior during elevated temperature fatigue.

Progression of microstructural damage was examined by interrupting fatigue tests at  $10^4$ ,  $10^5$ , and  $10^6$  cycles. These samples were tested at a maximum stress of 100MPa at 240°C. The microstructure of each sample was then observed for damage in the form of particle fracture.

## **2.6 Creep**

Creep tests were performed to compare the fracture behavior of the MMCs to both tensile and fatigue loading. Testing was performed in the same test frame used for tensile and fatigue samples. Samples were heated with the same induction heater used for both fatigue and tensile samples. Three stress levels, 69, 83, and 97MPa were tested at 240°C. These stress levels correspond to the mean stress in fatigue tests carried out in this study. All tests were run until sample failure by fracture.

## **2.7 Microstructural Examination**

Care was taken in sample preparation for microstructural examination to avoid damage to the reinforcing phases. Samples were sectioned with a slow speed diamond saw then mounted in Bakelite. Mounted samples were ground flat with 15µm diamond paper. Polishing with 6µm and 1µm diamond paste followed. Final polishing was achieved with .05µm alumina in water.

All fractured fatigue samples were sectioned perpendicular to the fracture surface to allow for examination of the microstructure near the fracture surface. Microstructures were observed near the fracture surface of sample to limit the effects of stress variation that occurs due to the hourglass sample geometry. For samples that did not fracture during testing, the center 25mm of the gauge was removed and sectioned transversely to the loading direction. All microstructural evaluation was done within 4.57mm of the

center of the sample. This ensured the stress in observed regions was at least 90% of the maximum stress experienced in the sample. The stress distribution of a fatigue sample relative to the maximum stress can be seen in Appendix B.

### 2.7.1 Particle Fracture

Particle fracture was examined by point counting. A grid of the approximate size of the SiC particles ( $15\mu\text{m} \times 15\mu\text{m}$ ) was placed over the microstructure with PaxIt! image analysis software and particles at intersections of the grid were classified as broken or unbroken. A broken particle was defined as one where at least one crack was seen to go through the entire particle. Particles that had fractured multiple times were counted once. Some large particles spanned multiple intersections, these particles were only counted once.

## 2.8 Temperature Control

To measure and control temperature during testing a sample was prepared with thermocouples along the gauge length and into the grip section of both a fatigue and tensile sample. Thermocouples were attached by drilling a blind hole in the sample. Figure 2.6 shows the location of all thermocouple attachment points for the fatigue sample. Thermocouples were then placed in the holes and held in place by peening the surface around the hole to pinch the thermocouple. This attachment technique was adopted from a NASA procedure for attaching thermocouples where other attachment methods are not ideal (Murtland et al. 2006). The instrumented sample was then heated in the same machine used for testing until the lower test temperature was reached and steady state was achieved. The process was repeated for the higher test temperature immediately after the lower test temperature. Steady state temperature profiles of the fatigue bar at both test temperatures can be seen in Figure 2.7.

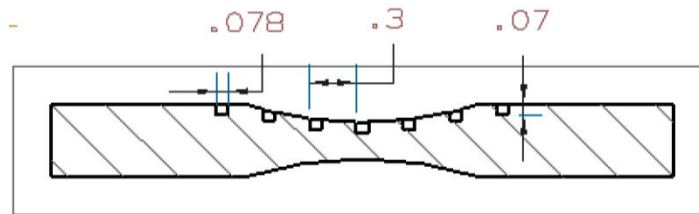


*Figure 2.6: Thermocouple locations for temperature distribution measurement (in).*

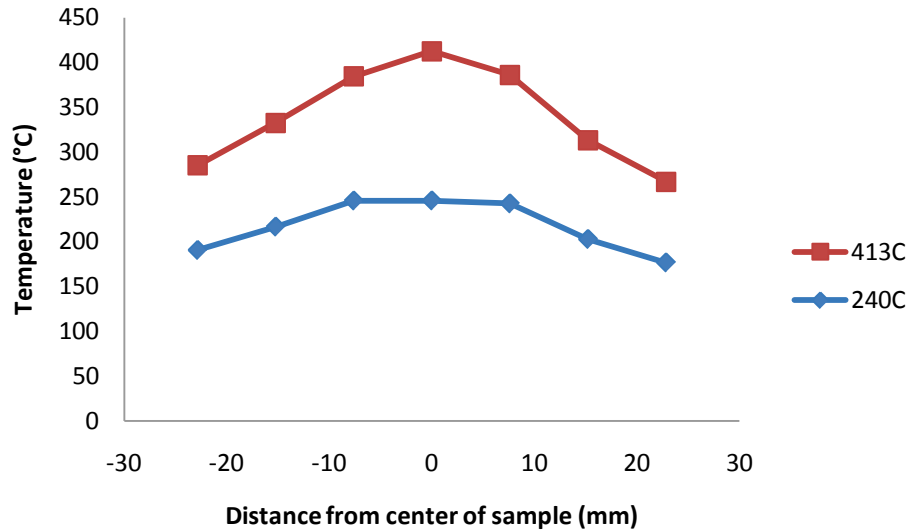


*Figure 2.7: Temperature profile of fatigue samples during induction heater on servo-hydraulic test frame used in this study.*

From this data, temperature set points were obtained where the temperature of the sample in the grip section could be controlled to achieve the correct test temperature in the center of the sample. Measuring temperature in the grip end of the sample avoided introduction of stress concentrators into the gauge length of the sample, which would have acted as crack initiation sites and affected the results. All samples tested had thermocouples in both grip ends to allow for control and monitoring of the sample temperature. Care was taken for all tests to ensure samples were in the same location relative to the grips and induction coil to limit temperature variability. Samples were placed in the grips so that the gauge section was 5.33mm (0.210in) from the grips on both ends of the sample. Temperature measurements were taken 3.05mm (0.120in) from the end of the gauge length on both ends of the sample. One thermocouple was used for controlling temperature while the other was used to monitor the temperature on an external system. A similar procedure was performed with tensile samples to obtain control set points for high temperature tensile and creep tests.



## 3. Results

### 3.1 Dwell Testing

#### 3.1.1 SiC-Matrix Interface

Optical microscopy showed no difference in SiC-matrix interface before and after high temperature dwell for either fiber type MMC. Figure 3.1 and Figure 3.2 show the microstructure of Saffil and Enfil samples before and after dwell testing at 240°C for 100 hrs. Backscattered electron imaging showed no evidence of interface reaction between SiC particles and the Al matrix at either test temperature.

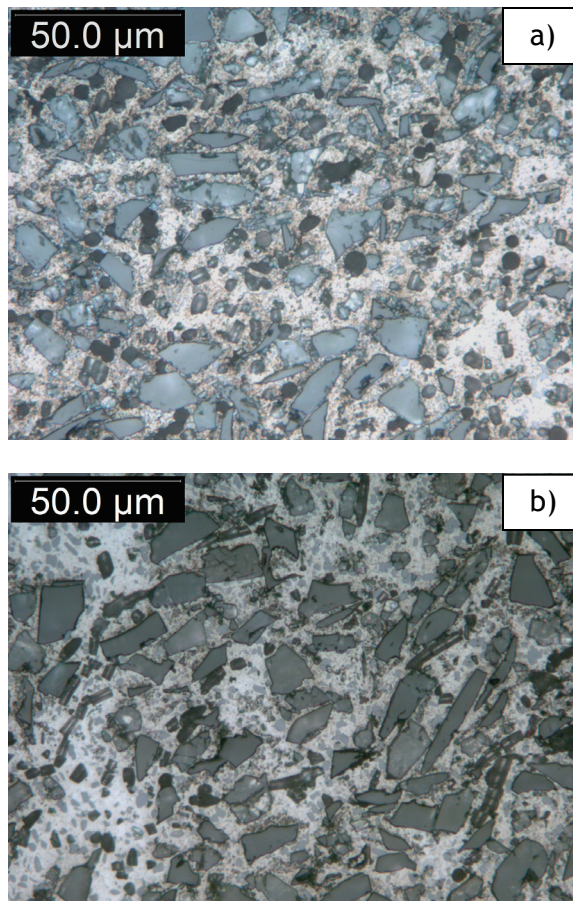


*Figure 3.1: Optical metallography of Saffil samples before (a) and after (b) dwell testing at 240°C for 100hr. No change in SiC-matrix or fiber matrix interface can be observed.*



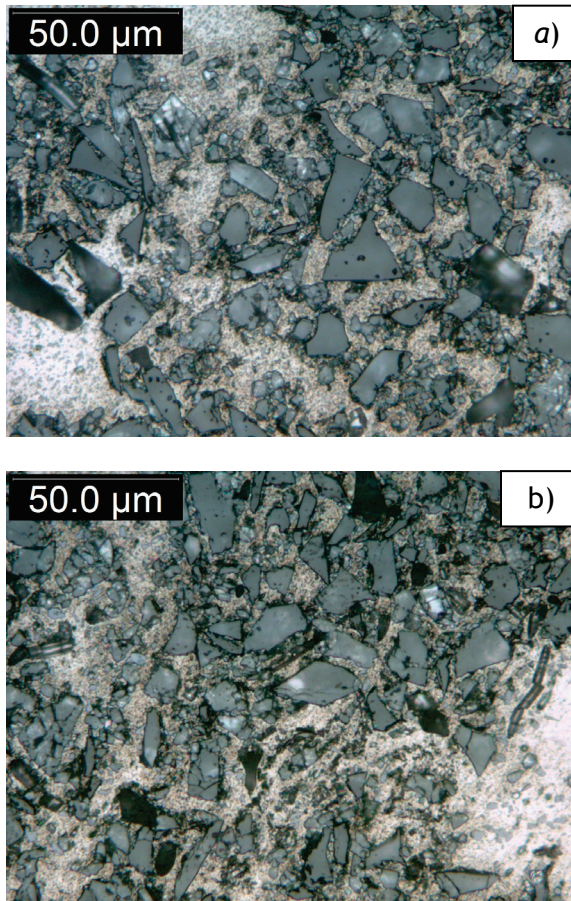


*Figure 3.2: Optical metallography of Enfil samples before (a) and after (b) dwell testing at 240°C for 100hr. No change in SiC-matrix or fiber matrix interface can be observed.*

The lack of pits and ledges from reactions between SiC particles and the matrix shows that there was no reaction between the SiC and the matrix. This is expected as SiC is stable in Al below the matrix solidus.

### **3.1.2 Fiber-Matrix Interface**

Optical and Backscattered Electron (BSE) examination of the microstructure showed no difference in the fiber-matrix interface after dwell testing in either fiber type MMC. BSE images of Enfil fiber MMC before and after dwell testing shown in Figure 3.3 show that the interface between matrix and fiber has not changed. It is possible that the if reaction products formed, they are too small to see in the SEM and would need to be evaluated in a TEM.

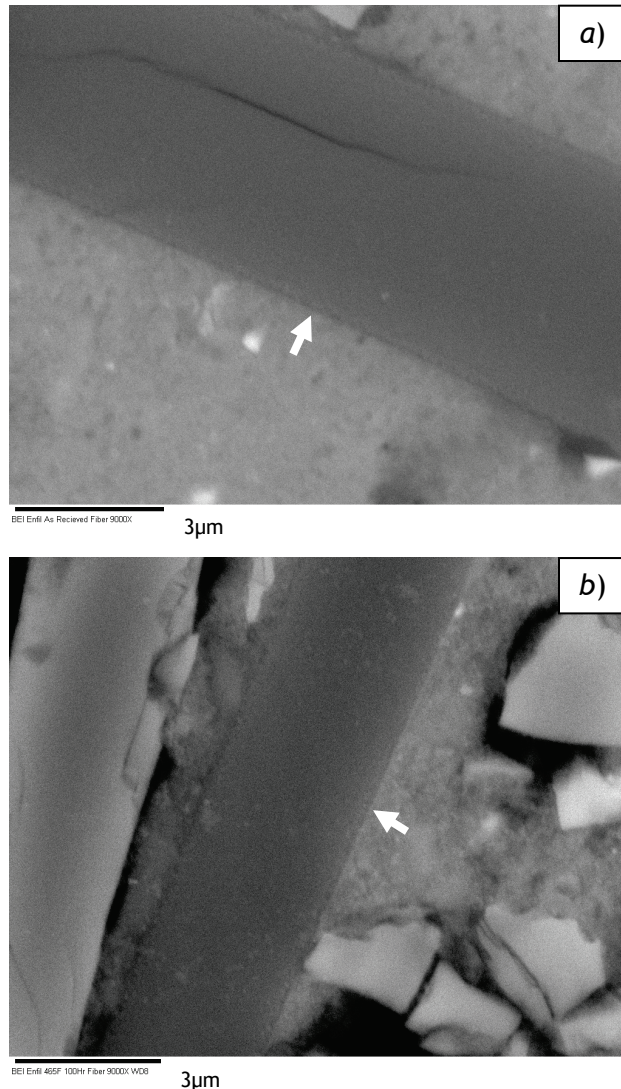


*Figure 3.3: Back Scattered Electron images of Enfil fiber MMCs before (a) and after (b) dwell testing at 240°C for 100hr. No evidence of an interface reaction can be observed either before or after temperature exposure.*

*(Arrows indicate fibers)*

### 3.1.3 Matrix Eutectic Si

It was observed that eutectic Si and or  $Mg_2Si$  in the A356 matrix underwent significant coarsening during dwell testing. This is expected as the dwell temperature is over the aging temperature of the alloy. This observed overaging will result in the mechanical properties of the matrix deteriorating over time. The reduced properties of the matrix can also negatively affect the properties of the composite. The microstructure of un-reinforced matrix regions can be seen in Figure 3.4. The precipitate structure after dwell testing results in poor mechanical properties.

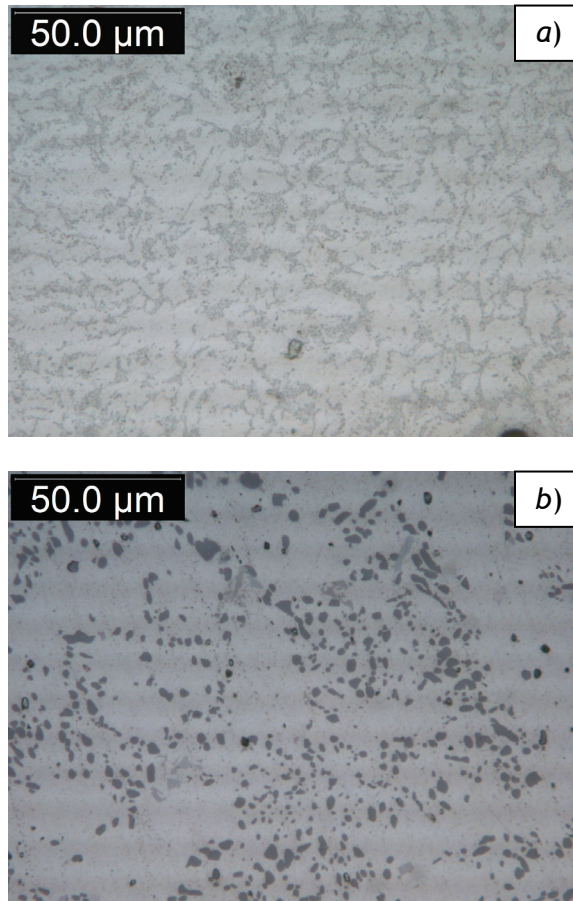


*Figure 3.4: Eutectic Si structure before (a) and after (b) dwell at 240°C for 100hr showing coarsening of eutectic Si particles.*

#### **3.1.4 Overall effect**

Dwell testing showed that there was no observable detrimental interface reaction layer forming in either composite during testing. The temperatures and times tested were not sufficient for the interface reaction to proceed in the solid state. Matrix eutectic Si size was the only observed microstructural change that occurred during dwell testing.

### **3.2 Elevated Temperature Tensile**

#### **3.2.1 Mechanical properties**

Tensile tests were performed at 240°C on Enfil and Saffil fiber MMCs as well as monolithic A356 from the same castings. Representative stress strain curves are shown in Figure 3.5, the results are summarized in Table 3.1. No tensile tests were carried out at 413°C. The modulus of both composites is much higher than the monolithic A356. Both the yield and ultimate tensile strength of the MMCs showed improvement over the matrix material. Necking

was observed in the monolithic A356 material, while none was observed for either MMC.

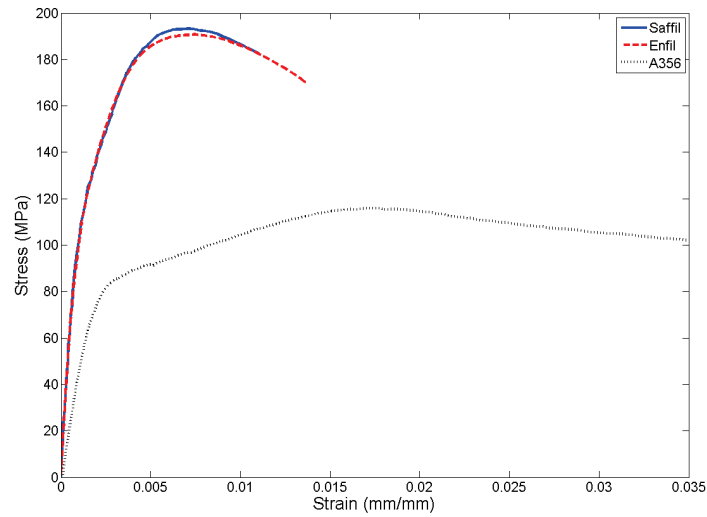


**Figure 3.5: Stress-Strain Curves for Enfil and Saffil MMCs and Monolithic A356 at 240 °C**

**Table 3.1**

*Tensile Properties of Enfil MMC, Saffil MMC, and monolithic A356 at 240 °C*

Material	Elastic Modulus (GPa)	Yield Strength (MPa)	Ultimate Tensile Strength (MPa)	Strain at failure (%)
Enfil MMC T5	122.6	90.9	190.7	1.37
Saffil MMC T5	98.32	94.7	181.6	1.10
Monolithic A356 T5	27.16	83.2	116.0	19.0

It should be noted that the reported properties are from samples with transversely aligned fibers. Properties measured along the long axis of the fibers are expected to be higher as the fibers are able to carry more load.



### 3.2.2 Fracture surface

Examination of the fracture appeared macroscopically brittle in nature. Figure 3.6 shows tensile fracture surfaces of both Saffil and Enfil fiber samples at low magnification. Few macroscopic features can be seen on the surface.

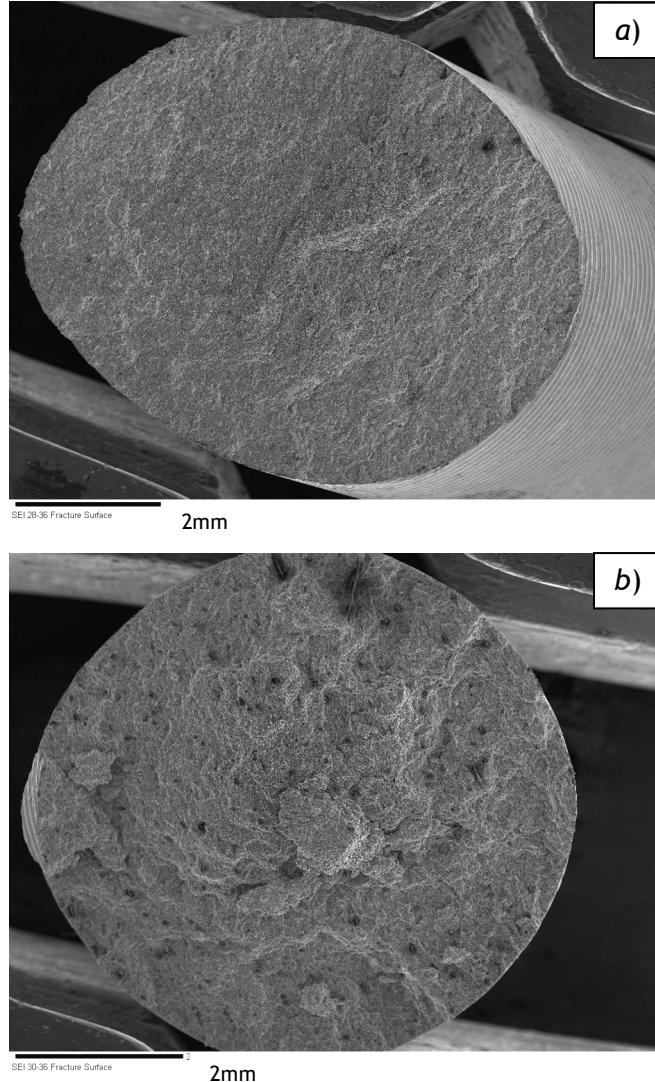


*Figure 3.6: Fracture surface of Saffil (a) and Enfil (b) tensile samples tested at 240°C. No regions of crack or growth can be observed. The fracture surface is macroscopically homogeneous.*

Closer evaluation of the fracture surfaces reveals that there are local regions of ductile and brittle failure as seen in Figure 3.7. Regions of brittle failure correspond to SiC particles while regions of ductile failure correspond to the matrix.

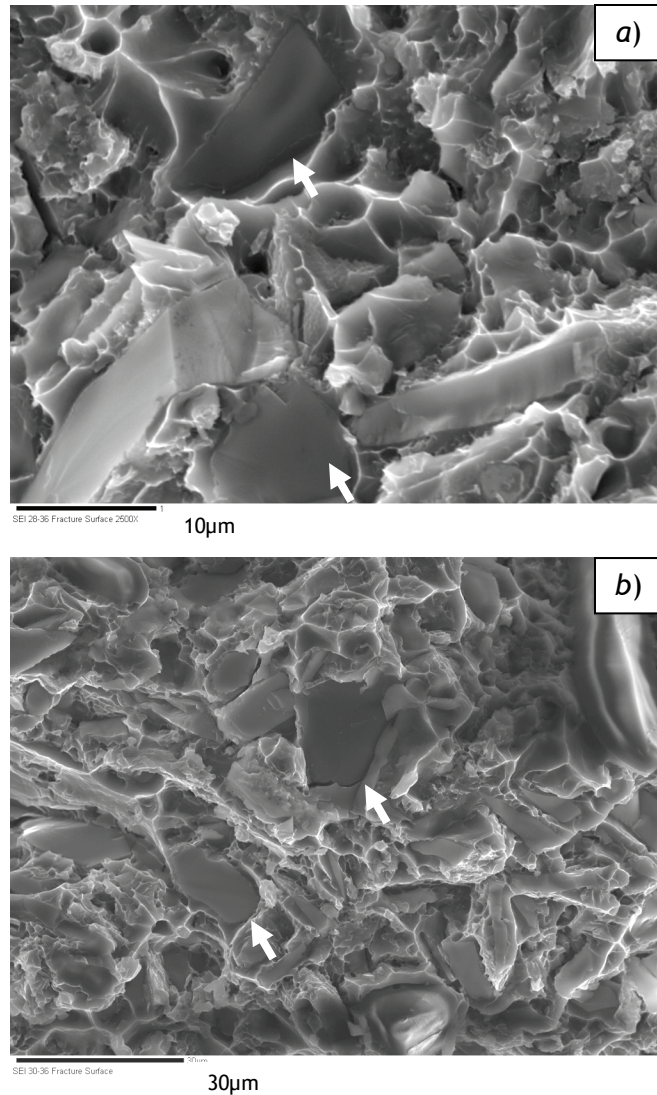


*Figure 3.7: High magnification fracture tensile fracture surfaces of Saffil (a) and Enfil (b) tested at 240°C. Regions of both ductile and brittle failure (arrows) can be seen. Brittle fracture occurs in SiC particles while ductile failure indicates failure in the matrix.*

By visual inspection, the particle content on the tensile fracture surface of both composites is similar to the bulk SiC volume fraction. This suggests that final failure of the sample does not occur preferentially in either the particles or the matrix.

### 3.3 Fatigue

Two Saffil MMC and one Enfil MMC samples tested at room temperature with a maximum stress of 240MPa were tested until run-out without failure. The decision was made to not run any tests at lower stress values as failure was unlikely to be observed.

Average S-N results for 240°C and 413°C are shown in Figure 3.8 and Figure 3.9 respectively. Representative fracture surfaces for all test conditions are shown in Figure 3.10. High magnification fracture surfaces are shown in Figure 3.11.

One Saffil and one Enfil sample tested at 240°C with a max stress of 100MPa were tested to run out without failure. This is unexpected as tests were performed in the low cycle fatigue regime at elevated temperatures. Variation of up to 80% was observed in fatigue life for all conditions tested. Full results from fatigue tests can be found in Appendix

At 240°C there was no clear pattern in which MMC had higher cycles to failure. At 140MPa maximum stress the Saffil MMC did not fail until one hundred thousand cycles after the Enfil MMC. The situation is reversed at both 120 and 100MPa with the Enfil MMC lasting longer than the Saffil MMC.

At 413°C the Saffil MMC had higher cycles to failure than the Enfil MMC at all maximum stress levels tested. At 120MPa maximum stress the Saffil MMC actually showed a reduction in cycles to failure compared to 100MPa maximum stress. The low cycles to failure at 413°C is due to the matrix being weak at that temperature. The test temperature is 75% of the homologous temperature of the matrix.

To determine if there is a statistically significant difference between Saffil and Enfil fiber MMCs, T tests were performed at each stress-temperature combination. The results for the T tests can be found in Appendix G: T-test for fatigue tests. It was found that for every situation where there was a significant difference between Enfil and Saffil fiber MMCs, the Saffil fiber MMC had higher cycles to failure. For samples tested at 413°C with a maximum stress of 140 and 100MPa there is no overlap in the observed failure range. This shows that there is a statistically significant difference in the mean value of cycles. If overlap is present, such as that observed for 240°C, maximum stress of 100MPa, there is doubt as to if the data sets came from parent distributions that are truly different.

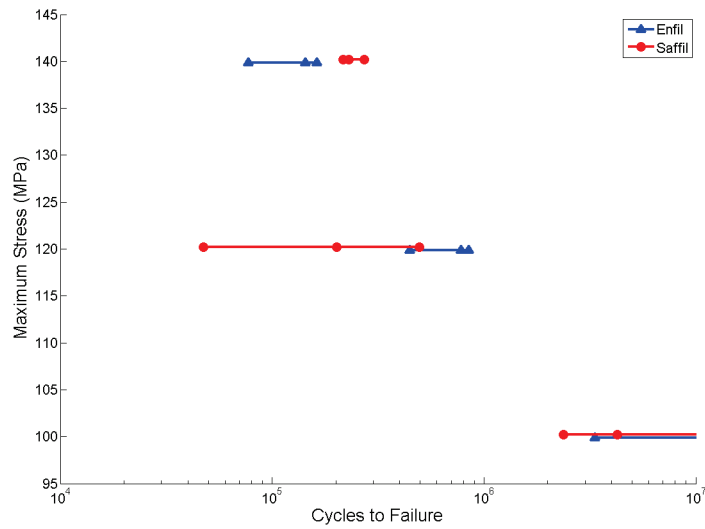


**Figure 3.8: 240 °C Fatigue Results for Enfil and Saffil MMCs**

*(Stress values for Saffil are vertically offset by 3.5MPa for ease of reading. Maximum stress levels were identical for both MMCs tested)*

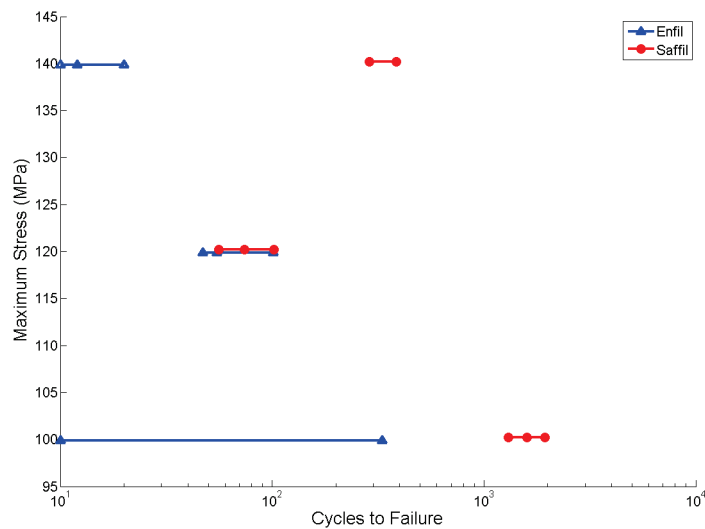


**Figure 3.9: 413 °C Fatigue Results for Enfil and Saffil MMCs**

*(Stress values for Saffil are vertically offset by 3.5MPa for ease of reading. Maximum stress levels were identical for both MMCs tested)*



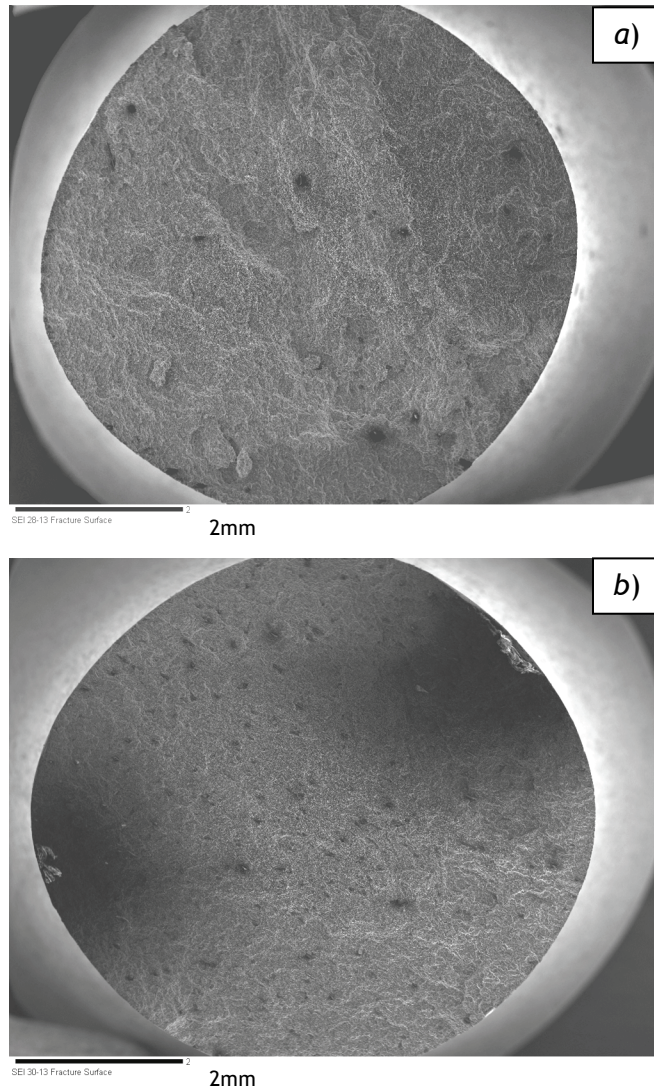


*Figure 3.10: Fracture Surfaces of Saffil (a) (maximum stress 140Mpa) and Enfil (b) (Maximum stress 120MPa) fiber fatigue samples tested at 240°C showing a uniform fracture surface with no indication of crack initiation and growth*

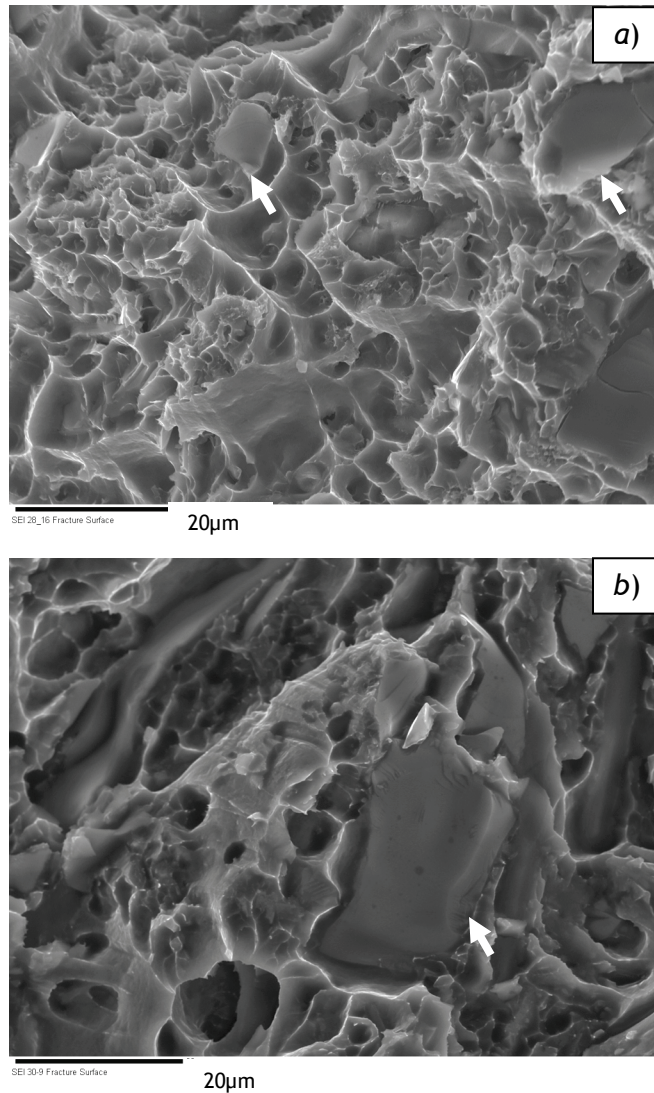


*Figure 3.11: High magnification images of Saffil (top) and Enfil (bottom) fiber samples tested in fatigue at 240°C with a maximum stress of 120MPa. Regions of both ductile and brittle failure (arrows) can be seen. Brittle fracture occurs in SiC particles while ductile failure indicates failure in the matrix. Fewer SiC particles are observed when compared to tensile fracture surfaces.*

Samples tested above room temperature failed on a plane not perpendicular to the loading direction. Failure often occurred on a single plane approximately 45° to the loading axis as shown in Figure 3.12 suggesting a shear mechanism is active during final failure. It was found that this failure was related to fiber orientation in the samples. Failure occurred on a plane parallel to the fiber orientation and along the plane of maximum shear from the externally applied stress. Figure 3.13 shows a schematic representation of

fiber orientation in test samples in relation to the plane of failure. Microstructures showing this orientation were shown in Figure 2.3. Microstructures viewed in both orientations from Figure 3.13 are shown in Figure 3.14.



*Figure 3.12: Fatigue sample failed on plane  $\sim 45^\circ$  to loading direction.*

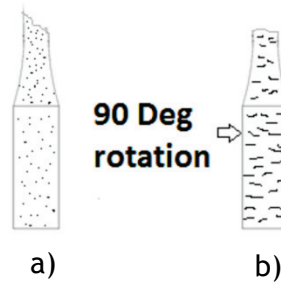


*Figure 3.13: Influence of fiber orientation on plane of failure. Samples failed on a plane parallel to the fiber orientation and approximately  $45^\circ$  to the loading direction.*

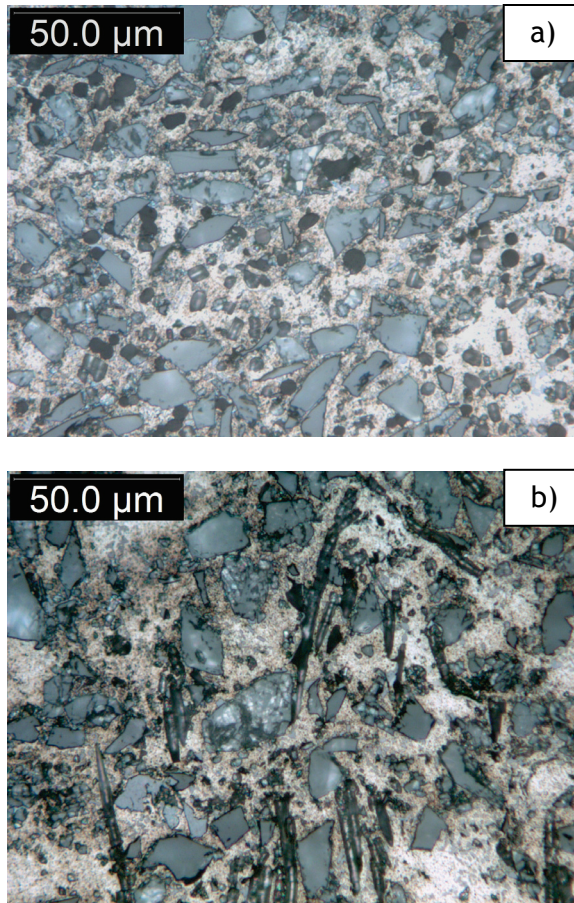


*Figure 3.14: Microstructure of fatigue sample viewed in plane a (a) and in plane b (b) from Figure 3.13 showing fiber orientation.*

At low magnification, fracture surfaces of fatigue samples were macroscopically brittle with few features. Fatigue fracture surfaces had a similar appearance to those observed in tensile tests.

Microscopically, regions of ductile and brittle failure were observed, with the majority of the surface appearing ductile in nature. The brittle failure regions corresponded to broken SiC particles, while ductile regions correspond to failure in the matrix. Hackle marks could be observed on SiC particles, as seen in Figure 3.15, indicating that particles fractured and have not de-bonded from the matrix. This indicates that the bond between particle and matrix is strong, further suggesting that the extent of interface reactions between the particles and the matrix is small. If particles were observed to de-bond from the matrix instead of fracturing it would mean that the interface is weak. No de-bonded particles were observed. No voids in the fracture surface where a SiC particle once was were observed in any sample examined.



This further suggests that there was good bonding between the SiC particles and the A356 matrix.

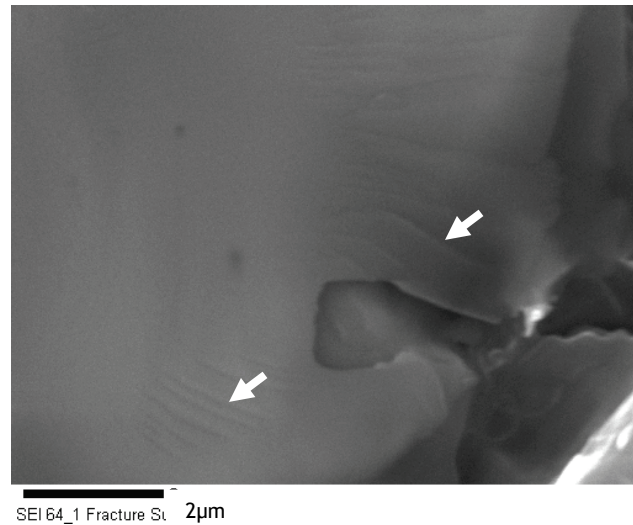


*Figure 3.15: Hackle marks on a SiC particle in a Saffil sample tested in fatigue at 240°C indicating brittle failure of the particle.*

*(Arrows indicate hackle marks)*

Samples tested in fatigue did not show the classic fatigue failure mode of cracks initiating, growing and leading to final failure. This is in contrast to results from other researchers who were able to identify regions of crack initiation and stable growth (Mkaddem and Mansori 2009). Failure in the current study appeared to occur due to overloading of the matrix. Fatigue fracture surfaces showed features that are similar to tensile fractures of the MMC with one key difference. Fatigue samples had a lower concentration of SiC particles on the fracture surface. This suggests that final failure of the composite occurred preferentially in the matrix, unlike tensile tests where final failure occurred in both particles and the matrix without a preference to one or the other.

### **3.4 Fiber content on fracture surface**

A higher content of fiber material was observed on the fracture surface of Enfil fiber samples. As seen in Figure 3.16, there are both fibers and shot particles present on the fracture surface of Enfil fiber samples. Shot particles and fiber were present in approximately the same ratio as the bulk composition of the MMC. Few of the observed shot particles or fibers were fractured. They had been pulled out of the other side of the fracture surface. This suggests that the interface is weaker than the shot particles and fiber for

the Enfil MMC. No SiC particle debonding was observed in either composite tested.

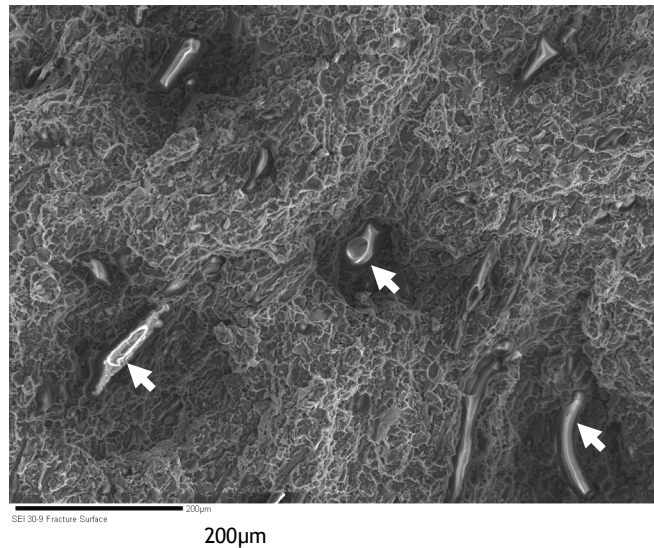


*Figure 3.16: Fiber and shot (arrows) on fracture surface of Enfil fiber MMC. Shot and fibers were observed in the same ratio that they are present in the bulk microstructure of the composite.*

Fibers were observed on the fracture surface of Saffil samples as well but not as frequently. As shown in Figure 3.17, where fibers and shot particles are seen as charged objects, there is a significantly higher presence of fiber on the fracture surface of Enfil samples. While the images in Figure 3.17 show creep fracture surfaces, the same behavior was observed in fatigue samples.

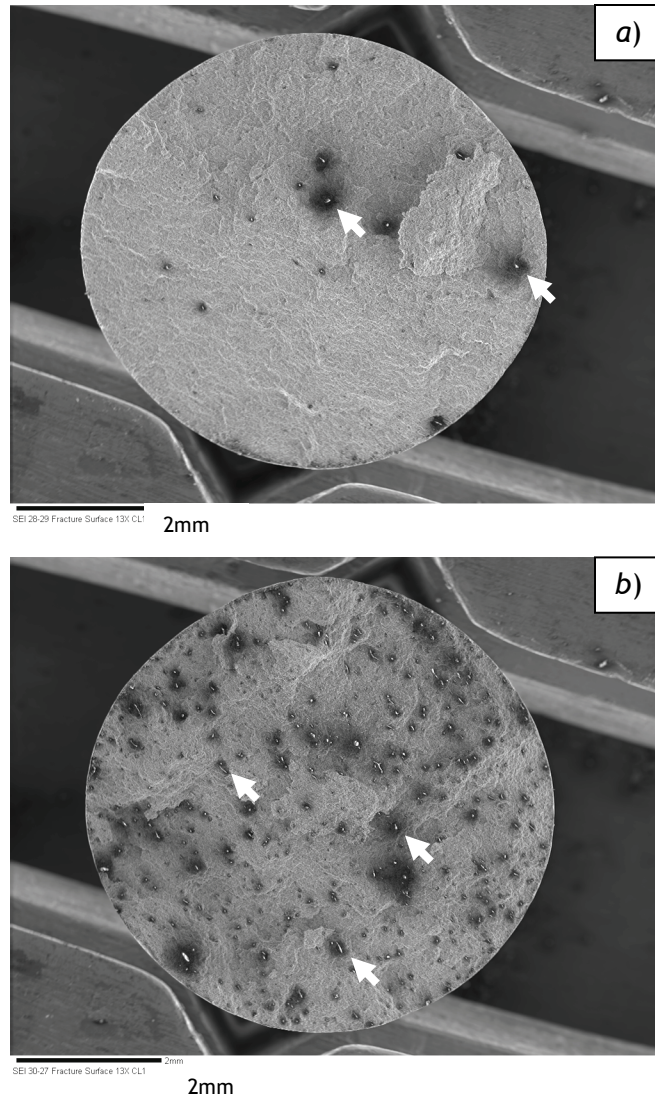


*Figure 3.17: Fiber content on creep fracture surface of Saffil (a) and Enfil (b) fiber MMCs tested at 240°C at a stress of 68.9MPa. Enfil fiber samples had a higher content of fibers on the fracture surface.*

*(Arrows indicate charged fibers/shot)*

The higher fiber (both fibers and shot particles) present on the fracture surface of the Enfil fiber samples suggests that the interface between Enfil fiber and the matrix is weaker than for Saffil fiber. This could be due to an interface reactions discussed earlier. The Mg in the matrix can react with silica present in the fiber to form a brittle spinel phase. Brittle phases between reinforcement and matrix have been found to result in poor mechanical properties. As discussed in section 3.1.2 no reaction products were observed during dwell testing. It is possible that any reaction products

were too small to see in the SEM. Reaction products as thin as 40 nm have been found to influence fracture (Evans 2003).

It is also possible that the interface between the matrix and Enfil is simply not as strong as that between Saffil and the matrix. Regardless of the reason for the lower strength interface, it represents a weakness in the material.

The effect of fiber interfacial strength will become more pronounced when fibers are aligned in the loading direction. Load is transferred to the fibers by shear forces between the matrix and fiber. If the interface is weak, it can break before the fiber is loaded to its maximum stress resulting in inefficient loading of the fiber.

### **3.5 Microstructure of fatigue samples**

#### **3.5.1 240°C testing**

Representative microstructures of samples tested at 240°C can be seen in Figure 3.18 and Figure 3.19. It was observed that there was significant damage to the SiC particles in all samples tested at 240°C. Damage occurred in the form of particle fracture. More damage was observed in samples that had a greater number of cycles to failure.

A few particles were observed to have fractured multiple times suggesting that even after a particle fractures once, it does not completely destroy its ability to carry load. It will however be significantly reduced. While it is possible that a particle fractures in multiple places at the same time it is unlikely to happen. A particle will fracture at its largest defect, where the critical stress to grow a crack is the smallest. Statistically it is unlikely to have two flaws in a particle that are exactly the same size, making it unlikely that a particle will fracture in two places at once.

It was also observed that the structure of the A356 matrix showed significant coarsening as seen in dwell testing. Unreinforced areas of fatigue samples showed coarsening similar to that shown in Figure 3.4. The increase in eutectic Si size will result in a decrease in ultimate tensile strength of the matrix.



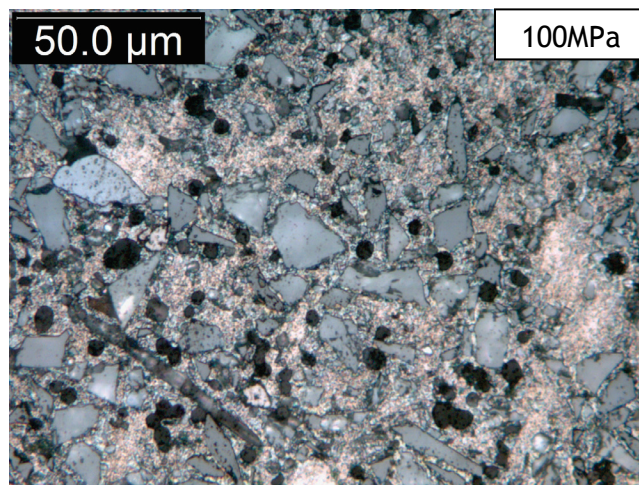
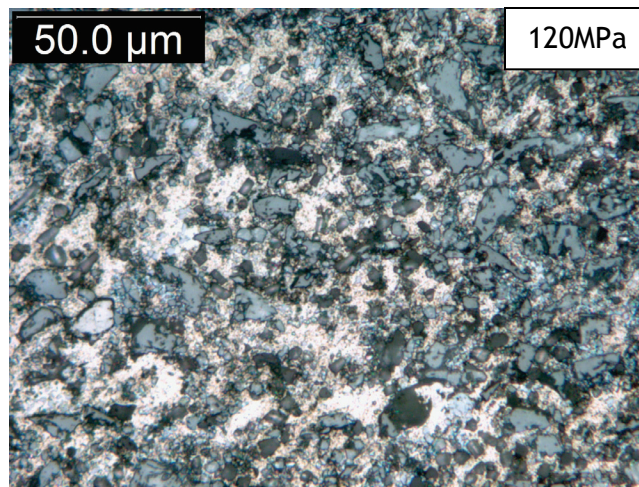
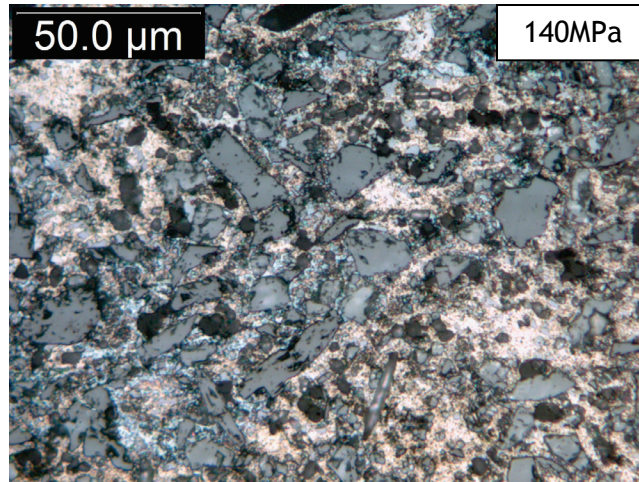


*Figure 3.18: Microstructure of Saffil samples after fatigue testing at 240°C. Damage to the composite can be seen in the form of SiC particle fracture*

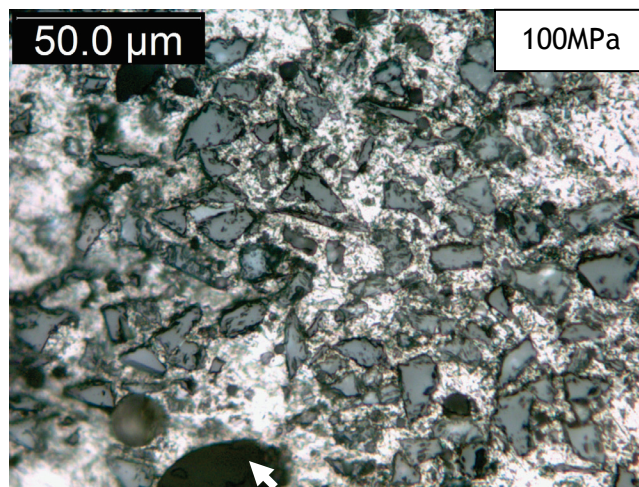
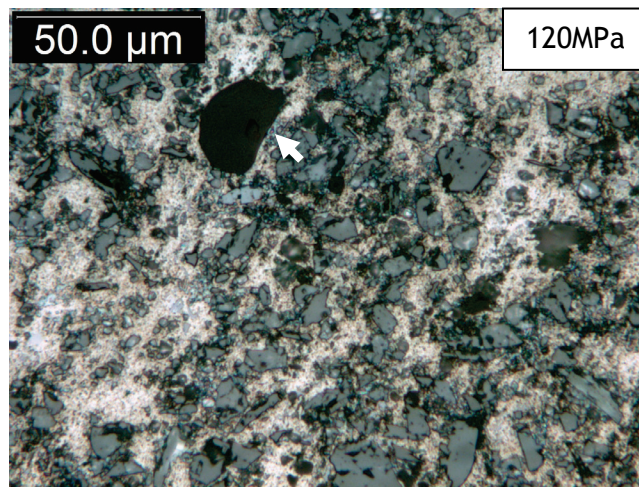
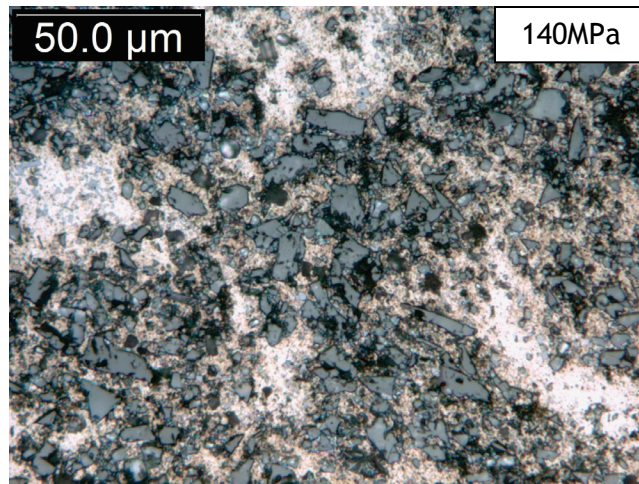


*Figure 3.19: Microstructure of Enfil samples after fatigue testing at 240°C. Shot particles present have not failed nor do they have cracks forming near them*

### **3.5.2 413 °C testing**

Representative microstructures of fatigue samples tested at 413 °C are shown in Figure 3.20 and Figure 3.21.

It can be seen that less damage has occurred in samples tested at 413 °C. The high test temperature results in a matrix that is too weak to load many particles to their failure stress before the matrix failed. Matrix coarsening was observed, but not to the extent seen in testing at the lower temperature. Test time was too short for coarsening to occur to the same extent.



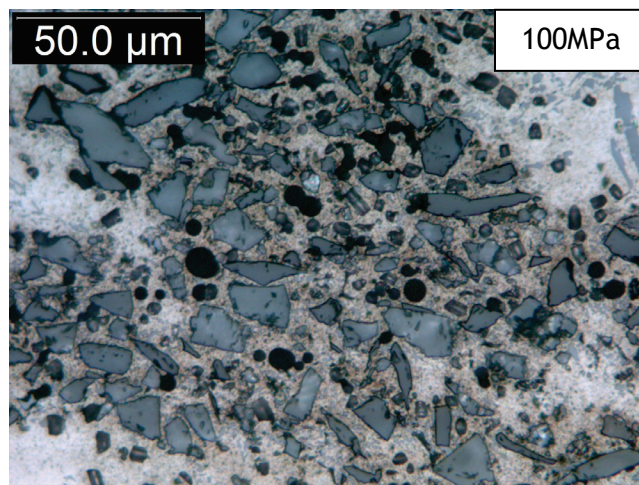
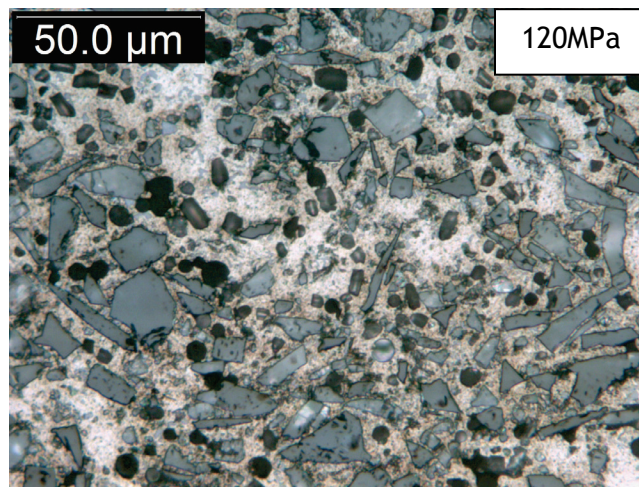
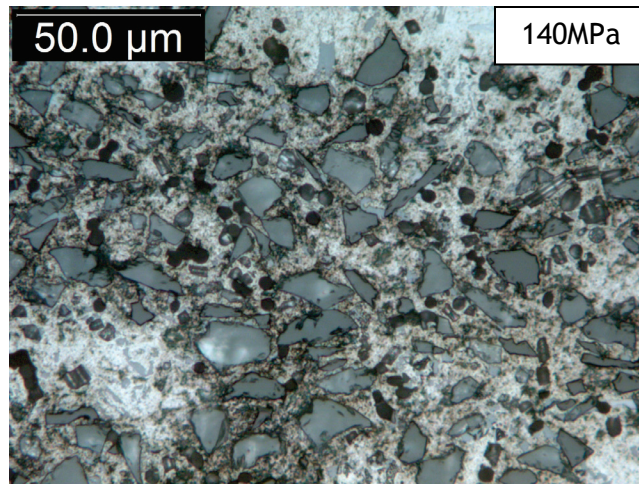


*Figure 3.20: Saffil samples after fatigue testing at 413°C. Fewer SiC particles have broken than in samples tested at 240°C*

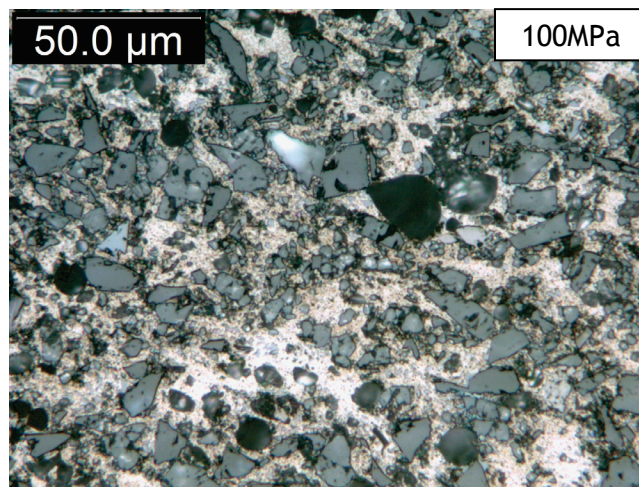
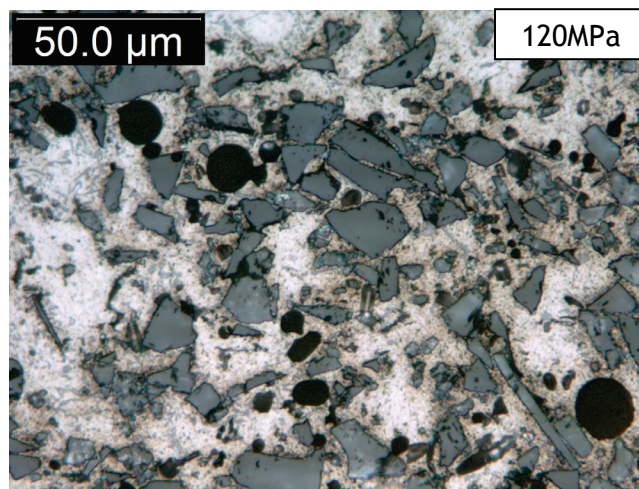
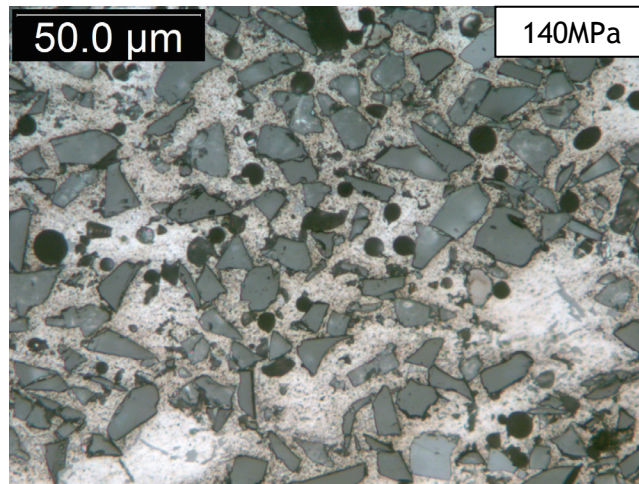


*Figure 3.21: Enfil fiber samples after fatigue testing at 413°C. Fewer SiC particles have broken than in samples tested at 240°C. No damage is seen to occur preferentially near shot particles.*

### 3.6 Particle Fracture Progression

Llorca found that the tensile failure in an aluminum 2618/15 vol% SiC composite was due to progressive particle fracture (Llorca 1993). It was found that large, high aspect ratio particles with major axis in the loading direction were fractured preferentially. Similar results were observed in this study. Large SiC have been fractured more often than smaller particles, with many large particles being fractured multiple times, Figure 3.22b. This suggests that particles are still able to carry some load even after they fracture.

Progressive fracture of SiC particles can also help to explain why the majority of final failure occurred in the matrix of the material. As particles fracture capacity to carry load is diminished, transferring the stress to the matrix. Eventually the load being applied is too great for the matrix to carry leading to failure. Microvoids are formed in the matrix near hard particles and coalesce resulting in the observed fracture surface showing microscopically ductile features. The few observed SiC particles are the last particles still carrying load that fracture.

Optical metallography of samples run to  $10^4$ ,  $10^5$ , and  $10^6$  cycles as well as an untested sample showed a progression of damage to the SiC particles in the form of cracking. Figure 3.22 shows the progression of particle damage in Saffil fiber samples. While as received samples showed 18% of the particles were broken, after 1 million cycles 55% were broken. The progression of particle fracture is shown in Figure 3.23. The last two points, at  $2.2 \times 10^6$  and  $4.3 \times 10^6$  cycles, are from failed samples tested at the same conditions. The particle fracture observed in these samples fits well with results observed in tests stopped before failure.



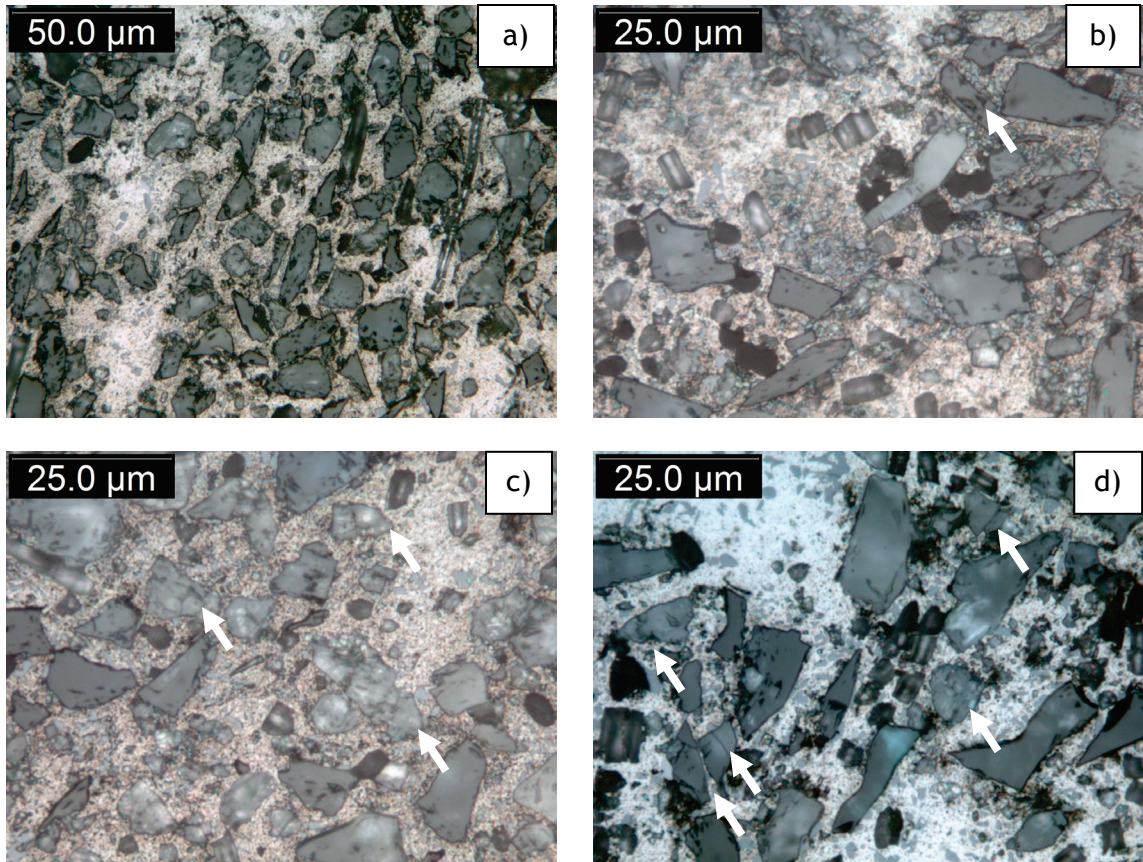


Figure 3.22: Microstructure of MMCs tested for 0 (a), 10,000 (b), 100,000 (c), and 1,000,000 (d) cycles with arrows indicating fractured particles. More particles have failed as the number of cycles increases.

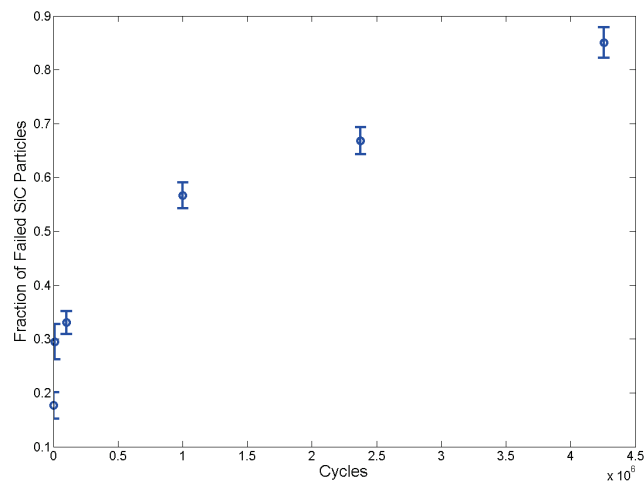


Figure 3.23: Particle fracture progression for samples tested at 240°C with a max stress of 100MPa. Fraction of failed particles for interrupted fatigue tests fits nicely with samples that were tested until failure

It can be observed that the rate of particle fracture is initially high but slows down as the number of cycles increases. This behavior can be explained by the variation in particle fracture stress due to particle size. Large particles have a lower fracture stress as described by the Griffith fracture criterion. As the large particles fail, a greater stress has to be applied to break the small particles.

### **3.7 Origin of dimples on fracture surface**

Since many particles have fractured during fatigue testing and most of the load is carried by the matrix, final failure of the composite will occur in the matrix. Examination of the fatigue fracture surface shows that the presence of SiC particles on the fracture surface is much lower than the bulk composition of the composite.

The origin of the cup and cone type failure observed in ductile materials is often a hard particle in the material (Gurland and Plateau 1963). This can be a precipitate in a monolithic metal, or a reinforcing particle in a MMC. The presence of the hard particle results in high stress in the matrix near the particle. The high stress results in large amounts of deformation near the particle. As deformation continues, microvoids coalesce and form voids that grow leading to the characteristic dimpled appearance. If the dimples come from SiC particles, the spacing of the dimples will be about the same as the spacing of SiC particles.

In this study however, the spacing of the dimples was found to be much smaller than the size of the reinforcing particles. Dimple spacing was found to be on the order of 5  $\mu\text{m}$  while the average size of SiC particles is 35  $\mu\text{m}$  which gives them a spacing of 50  $\mu\text{m}$ . Figure 3.24 shows a number of dimples in the matrix near a fractured particle showing the dimple spacing is much smaller than a SiC particle. This suggests that the dimples observed on the fracture surface are not related to the presence of SiC particles. It was observed that the spacing of precipitates in the matrix is near 5  $\mu\text{m}$ . It is likely that the dimples observed on the fracture surface are the result of large amounts of plastic deformation around eutectic Si particles in the matrix.



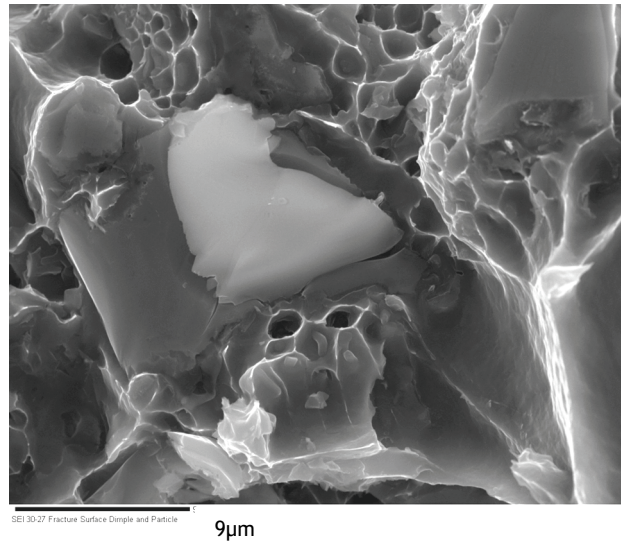


*Figure 3.24: Fractured SiC particle and dimples in the matrix. Multiple dimples can be seen that are closer together than the size of the SiC particle.*

### **3.8 Component role in final failure of composite**

Table 3.2 summarizes each component in the composites role in the final failure of the material in fatigue. Based on these results it was determined that overageing of the matrix and progressive fracture of SiC particles were the most important mechanisms controlling final failure. The presence of fibers and shot particles added little to the strength of the composite and appeared to have small influences on when the composite failed in fatigue.

Table 3.2

*Composite component role in final fatigue failure*

Component in composite	Volume Fraction	Role in final failure of composite in fatigue
Fibers	0.05	<ul style="list-style-type: none"> <li>• Failure occurs on a plane parallel to fiber alignment direction</li> <li>• Many fibers are present on the fracture surface of the Enfil MMC</li> <li>• Fewer fibers are present on the fracture surface of the Saffil MMC</li> </ul>
Shot particles	0.002	<ul style="list-style-type: none"> <li>• Shot particles are present on the fracture surface in a similar ratio to fibers in the bulk composite</li> <li>• Few shot particles are observed to be broken on the fracture surface</li> </ul>
SiC Particles	0.35	<ul style="list-style-type: none"> <li>• Volume fraction of failed particles is observed to increase as number of cycles increases</li> </ul>
Matrix	Remain	<ul style="list-style-type: none"> <li>• Eutectic Si coarsening is observed in samples tested at 240°C</li> <li>• Overageing decreases matrix UTS as testing progresses</li> <li>• Dimple spacing on fracture surface is similar to spacing between eutectic Si particles</li> </ul>

### 3.9 Creep

Creep tests were carried out to compare the failure mechanisms observed in fatigue to determine similarity. Results are shown in Table 3.3. In general, strain to failure and time to failure increased with decreasing stress.

*Table 3.3*  
*Creep Results at 240 °C*

Fiber	Stress level (MPa)	Time to failure (Hr)	Strain at Failure (%)
Saffil	96.5	0.52	2.10
Saffil	82.7	3.80	1.85
Saffil	68.9	14.90	2.44
Enfil	96.5	2.71	1.01
Enfil	82.7	0.77	2.13
Enfil	68.9	10.54	2.31

Fracture surfaces of creep and fatigue samples were compared and found to be similar. Figure 3.25 shows a side by side comparison of creep and fatigue tests with the same mean stress values carried out at the same temperature. Both show regions of ductile and brittle failure with the majority of final failure occurring in the matrix.

Creep tests lasted significantly shorter times than fatigue tests at the same mean stress. This suggests that while the final failure mechanisms are similar, in the appearance of the fracture surfaces, they are not the same. Microstructures of both Saffil and Enfil MMCs after creep testing at 68.9Mpa, Figure 3.26, show that there are few fractured SiC particles. Less than 10% of the SiC particles have been fractured during creep testing, compared to upwards of 70% during fatigue testing at the same temperature and mean stress.

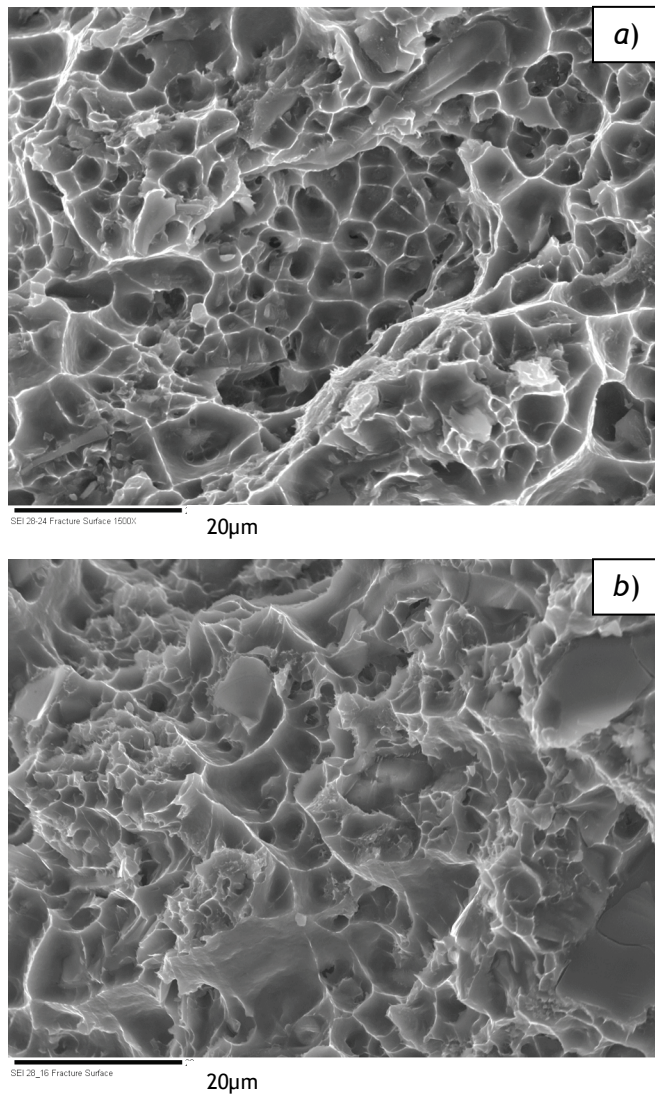


*Figure 3.25: 82.7MPa creep (a) and 120MPa fatigue (b) fracture surfaces tested at 240°C. Mean stresses for both samples was identical. Fracture surfaces are similar in appearance with regions of both ductile and brittle failure.*

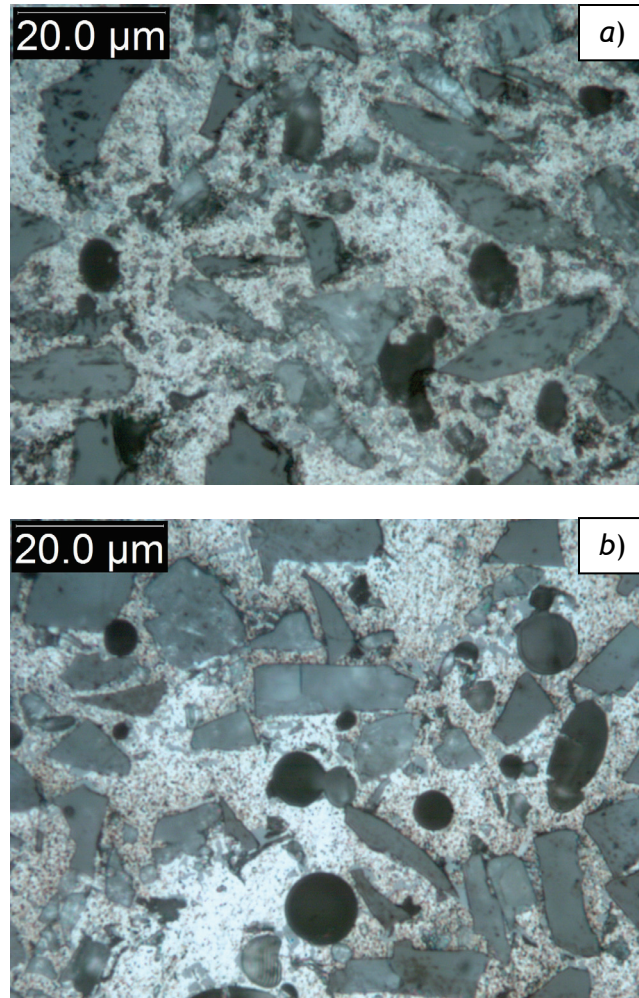


*Figure 3.26: Microstructure of Saffil (a) and Enfil (b) samples after 68.9MPa creep testing at 240°C. Few SiC particles tested in creep fractured.*

The difference in fraction of fractured SiC particles is likely due to the cyclic strain experienced by those particles tested in fatigue. In creep, the matrix is allowed more time to flow around the particles, the dynamic nature of the stress-strain state in fatigue does not allow for as much flow by the matrix to relieve the strain experienced by particles. This results in higher stresses in the particles and subsequently more of the SiC particles fracture during fatigue testing. The high strain rate in fatigue also impacts dislocation behavior. Dislocations in the matrix do not have as much time to move, this results in higher matrix strength. A higher strength matrix is more likely to cause particle fracture (Hall et al. 1994).

## 4. Discussion

Final failure of the composite in fatigue at high temperature occurred mainly in the matrix. Fibers appeared to play a minimal role in when the composite failed in the Saffil fiber reinforced composite. It was observed that the fraction of broken SiC particles increases as testing progresses, forcing the matrix to carry a greater load. To test if failure in the composite is a result of matrix overloading, a model was developed based on the work of previous researches who have examined modeling of the tensile behavior of MMCs.

### 4.1 Modeling

#### 4.1.1 Observed particle fracture

An effective medium approach, developed by Corbin and Wilkinson to predict the tensile behavior of a composite, was applied to predict failure in fatigue. The original model calculates the tensile response of a composite based on the stress strain curves of all components (SiC and matrix metal) in the system. It is assumed that the particles are perfectly elastic as SiC is a brittle ceramic that does not yield before it fractures. The stress-strain curve of the matrix material at 240°F was obtained from a tensile test to allow for calculation of an instantaneous matrix modulus.

A Ramberg-Osgood relationship, as shown in equation 4.1 was fitted to the stress strain curve of the matrix for ease of computation. A Matlab, version 7.10.0, program, found in Appendix F: Additional Matlab functions, was used to fit the parameters  $\alpha$  and  $N$  to the experimental A356 matrix stress strain curve. Values of  $\alpha$  and  $N$  were found to be 0.0146 and 0.1053 respectively.

$$\epsilon = \frac{\sigma}{E} + \alpha \frac{\sigma^Y}{E} \left( \frac{\sigma}{\sigma^Y} \right)^{\frac{1}{N}} \quad (4.1)$$

To simplify calculations, the composite was assumed to be comprised only of the matrix and SiC particles. Fibers were ignored as they are transversely aligned to the loading direction for all samples tested. Fibers in this orientation add little to the strength of the composite as they are not able to fully load. Shot particles were also ignored as they comprised a small fraction (0.2%) of the volume of the composite if they were present. Rule of mixture calculations show that by ignoring fibers and shot, the predicted modulus of the composite is reduced by 10% and more closely matches the observed modulus values.

Table 4.1

*Experimental and rule of mixtures elastic modulus for Saffil fiber MMC at room temperature*

Modulus Type	Elastic Modulus (GPa)
Experimentally observed	131
Rule of mixtures (including fiber)	202
Rule of mixtures (ignoring fiber)	191

SiC particles were assumed to be uniformly distributed spheres. Any strengthening due to Orowan dispersion effects was ignored as the particles are so large and present in such a high volume fraction that the center to center spacing between particles is large (50 $\mu$ m). Poisson's ratio for the matrix of was assumed to be 1/2. These assumptions were the same used by Corbin and Wilkinson for their model. With these assumptions, the stress in a particle of each phase, A356 matrix and SiC particle, can be calculated by equations 4.2 and 4.3 (S.F. Corbin 1993).

$$\sigma^r = \left( \frac{5E_r}{2E_r + 3E_c} \right) \sigma^c \quad (4.2)$$

$$\sigma^m = \left( \frac{5E_m}{2E_m + 3E_c} \right) \sigma^c \quad (4.3)$$

Where  $\sigma^r$  is the stress experienced by a particle of the reinforcing phase,  $\sigma^m$  is the stress experienced in the matrix and  $\sigma^c$  is the stress applied to the composite.  $E_r$  and  $E_m$  are the instantaneous reinforcement and matrix moduli, respectively. The modulus of SiC is assumed to be constant because it fractures before it yields. The matrix can plastically deform so the instantaneous modulus is not constant. Therefore an instantaneous modulus was calculated using the stress-strain curve of the matrix. With the modulus values of the component phases the modulus of the composite can be found with equation 4.4.

$$3E_c^2 + [(2 - 5V_r)E_r + (2 - 5V_m)E_m]E_c - 2E_rE_m = 0 \quad (4.4)$$

Where  $E_c$  is the composite modulus and  $V_{r,m}$  are the volume fraction of the reinforcement and matrix respectively. The stress-strain behavior of the matrix as assumed to be constant throughout the test for the purpose of

calculating the composite stress-strain behavior. No over aging effects were taken into account in calculating the stress-strain behavior for this model.

For this study, model was modified to account for particle fracture by assuming that once a particle fractures, it is no longer able to carry any load. Once a particle is broken, it is treated effectively as a pore in the material. This approach of treating a broken particle as a pore is similar to how particle fracture has been treated in the calculation of a tensile curve (Nan and Clarke 1995). The fraction of fractured particles at a given cycle was obtained from experimental results (Figure 3.23) and subtracted from the nominal particle volume fraction.

The procedure outlined in Figure 4.1 was used to calculate the composite stress strain curve. This process was repeated for each cycle varying the volume fraction of particles present according to experimental observation. The matrix volume fraction was kept constant. The maximum matrix and reinforcement stress in a cycle, as calculated by equations 4.2 and 4.3, were tabulated and plotted (Figure 4.2).



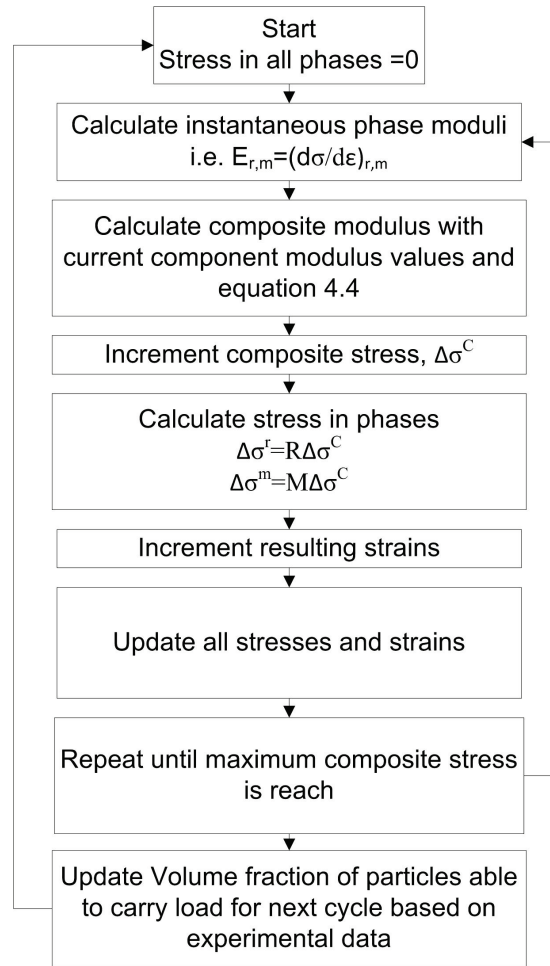


**Figure 4.1: Procedure for calculating composite stress strain curve**

*(note:  $R$  and  $M$  are the constants from equations 4.2 and 4.3 respectively)*

The failure criterion for the composite was defined as the point where the stress in the matrix exceeded the ultimate tensile strength (UTS) of the matrix. To account for matrix softening due to over aging, a curve for matrix UTS was fitted to tensile data of A356 held at high temperature for varying times (Brosnan and Shivkumar 1995). The ultimate tensile strength as a function of time at 240°C is shown in Table 4.1. The UTS curve was plotted on the same axis as the maximum matrix and reinforcement stresses.

Table 4.2

*Ultimate Tensile strength of A356 as a function of time at 240°C*

Time (hr)	Ultimate Tensile Strength (Mpa)	Fraction of maximum strength
0.5	117.13	1.00
10	103.35	0.88
100	89.57	0.76
1000	82.68	0.71
10000	68.9	0.59

The described approach was executed using a Matlab, version 7.10.0, program. The code used for calculating the maximum stress in both phases based on experimentally determined particle fracture can be found in Appendix 4: Model Code for observed particle fracture.

The model was used to examine the fatigue performance of a composite tested at 240°C at a maximum stress of 100MPa, the lowest stress condition tested experimentally. This was found to be the most interesting condition tested as it had a large number of cycles to failure. This allowed for measurement of particle fracture progression over a large number of cycles. Maximum stresses in both the matrix and reinforcement particles calculated by the model described in Figure 4.1 are plotted in Figure 4.2, along with the matrix UTS. It can be shown that the model predicts failure at approximately 2.5 million cycles. Actual failures occurred at 2.4 and 4.3 million cycles. It should also be noted that one sample tested at these conditions ran out to 11.5 million cycles.

As SiC particles fracture, a higher stress is experienced in unbroken particles this accommodates the constant maximum stress applied during each cycle. As particles fracture and no longer carry any load, the matrix is forced to carry a portion of the stress that was once carried by the SiC particles. This increase in load is seen as the increase in max matrix stress. The matrix stress increases until all of the particles have failed. At this point the particle stress goes to zero and the matrix carries all of the load.

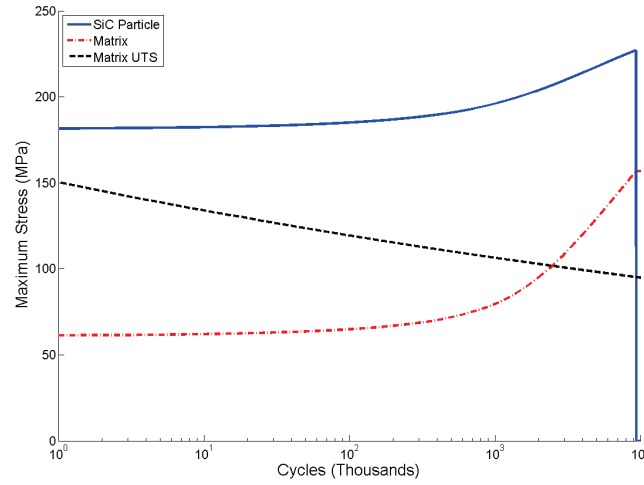


*Figure 4.2: Maximum stress in matrix and SiC particles and matrix UTS as calculated by the model based on observed particle fracture. Failure is predicted at 2.5 million cycles.*

#### 4.1.2 Calculating particle fracture

The above model is dependent on feeding in particle fracture data. However particle fracture rate is dependent on temperature (affecting matrix tensile behavior) and fatigue cycle stress level. To make the model a more powerful predictive tool, an attempt to calculate particle fracture was made. A Weibull strength distribution was applied to the SiC particles while assuming the particles are identical in volume. Matrix yielding and recovery were accounted for. Composite creep was also included to more accurately calculate particle fracture. It was assumed that the UTS of the matrix will not be affected by work hardening and will follow the same softening behavior observed in Table 4.1.

#### 4.1.3 Particle Strength Distribution

Silicon Carbide particles have a distribution of flaws, both size and type, in them. The flaw with the greatest stress concentration will cause a SiC particle to fail. The fracture strength of ceramics often follow a Weibull type distribution where the probability a particle will survive an applied stress is given by:

$$Ps = \exp \left[ - \left( \frac{\sigma}{\sigma_0} \right)^m \right] \quad (4.5)$$

Where  $\sigma$  is the applied stress to a particle,  $\sigma_0$  is a reference strength for the material being tested, in this work  $\sigma_0$  was assumed to be 1850MPa (Snead,

et al. 2007). The Weibull modulus,  $m$ , gives an idea of the distribution of flaw sizes in a material. For this work, a value of 1.05 was used for the Weibull modulus to fit the results to experimental observations. Typical Weibull modulus values for SiC range from 3-11 (Snead, et al. 2007). A high Weibull modulus means that the material has a narrow flaw size distribution, while a low modulus value suggests a wide distribution of flaw sizes. The Weibull modulus is affected by flaw type. Surface and interior flaws will have different modulus values, it is possible that the process for manufacturing SiC particles additional flaws were introduced. Surface flaws could have formed on the SiC creating a situation where multiple flaw types exist which has the potential to lower the Wiebull modulus.

#### 4.1.4 Matrix Yielding

The model was also modified to account for work hardening in the matrix by replacing the Ramburg-Osgood equation with one that accounts for work hardening:

$$\sigma = \sigma_y + K\epsilon_p^n \quad (4.6)$$

Where  $K$  is the strength index,  $n$  is the strain hardening exponent and  $\epsilon_p$  is the plastic strain. In this work values of 8000 for  $K$  and 0.2 for  $n$  were used. If the matrix stress in a cycle exceeded the yield stress as described in equation 4.7 the yield stress of the matrix for the next cycle was increased to that maximum stress observed in the cycle.

#### 4.1.5 Matrix Recovery

The assumption was made that the matrix will recover during testing. The high temperature seen during testing will allow dislocations in the matrix to reorder and combine to lower the energy of the system. For this work, it was assumed that the matrix recovered 90% of the strain that occurs during each cycle at 240°C.

#### 4.1.6 Composite Creep

The high temperature and stress state of fatigue testing in this study will lead to creep occurring in the composite. Average total displacement of a sample in fatigue, shown in Figure 4.3, was found to increase by 1.59E-8 mm per cycle. Average displacement is the mean displacement of sample as a function of cycles. Stroke is defined as the distance the actuator had to move to apply the load to the sample (maximum position-minimum position). The stroke is also plotted in Figure 4.3 and is effectively constant. All data for

Figure 4.3 was collected by recording the position of the hydraulic actuator during testing.

Observed deformation is assumed to be entirely due to creep as any deformation due to yielding is expected to be four orders of magnitude larger. Calculations for deformation due to yielding can be found in Appendix F: Displacement due to plastic strain from yielding. The rate of deformation is assumed to be approximately equal to the strain rate of the composite during fatigue testing. While strain in the sample is not uniform due to the hourglass shape, it is assumed that the majority of deformation will occur in the middle of the gauge length.

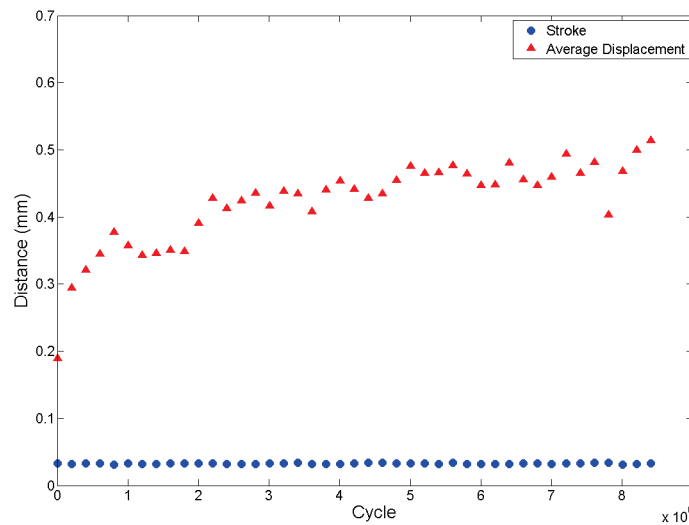


*Figure 4.3: Average actuator displacement and stroke for fatigue test with maximum stress of 100MPa at 240°C showing an increase in displacement with cycles.*

The increased displacement per cycle results in a creep strain rate of 1.25E-8 per hour. This is about an order of magnitude lower than the creep rate observed for the composite at the same temperature and mean stress.

#### 4.1.7 Numerical Method

It was assumed that there was no slippage at the matrix-particle interface when there was plastic deformation of the matrix. This assumption leads to the plastic strain experienced by the matrix, from either matrix yielding or creep, being stored in the particles, increasing the stress in the particles at the beginning of the next cycle.

The stress strain behavior of the composite was then calculated for each cycle as described in Figure 4.4.

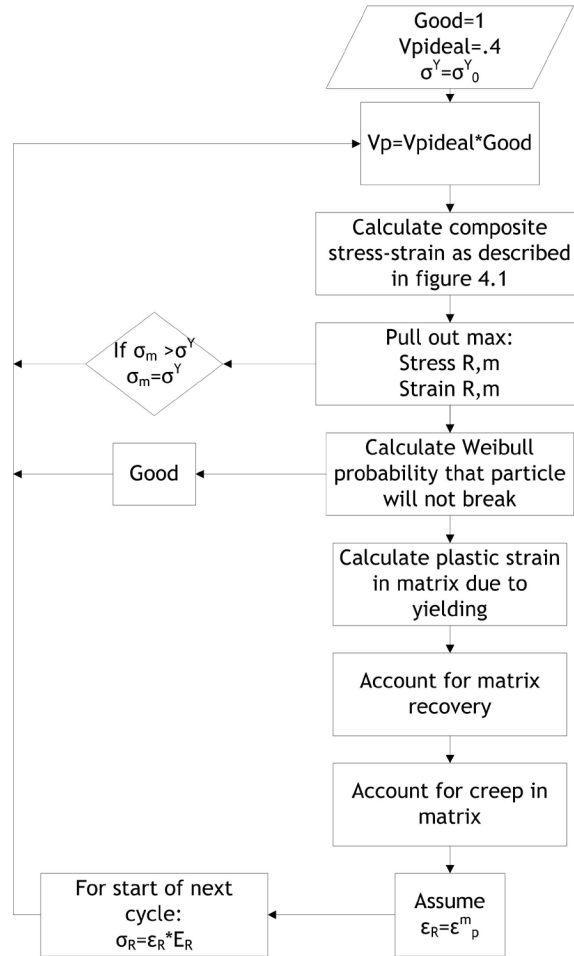


*Figure 4.4: Method used to calculate fatigue behavior of composite based on calculated particle fracture.*

The described approach was executed using a Matlab, version 7.10.0, program. The code used for calculating the maximum stress in both phases based on calculated particle fracture data can be found in Appendix D: Model code for calculated particle fracture.

By following the procedure outlined in Figure 4.4, and using the Weibull modulus and recovery rate as fitting parameters, the volume fraction of particles able to carry load was calculated and is shown in Figure 4.5. The model results in a reasonably good fit for the volume fraction of un-fractured particles.

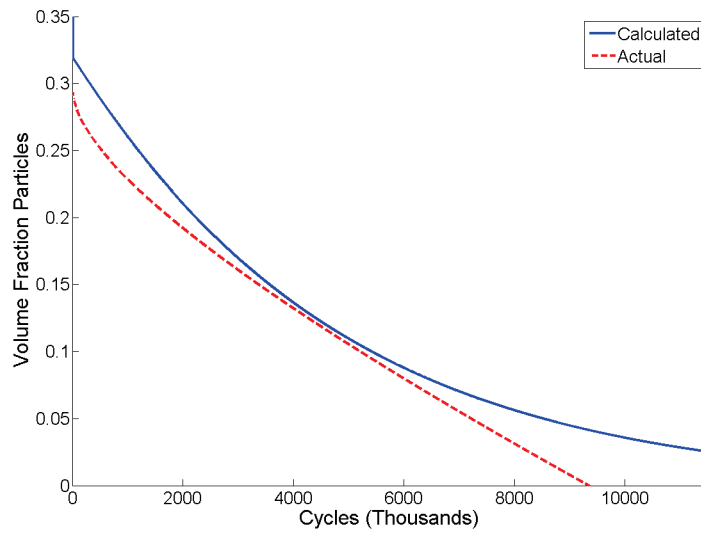


*Figure 4.5: Calculated and observed SiC particle volume fraction for testing at 465 °F with a maximum stress of 100MPa.*

Maximum stresses experienced in all phases based on the calculated particle volume fraction are shown in Figure 4.6. Since the volume fraction of particles carrying load is similar to that observed experimentally, the stress experienced in the matrix is also similar. The ultimate tensile strength of the matrix is exceeded after approximately 4.8 million cycles. This is slightly higher than the observed failure range of 2.5 to 4.3 million cycles. However, one sample tested at this condition ran out to 11.5 million cycles without failure.

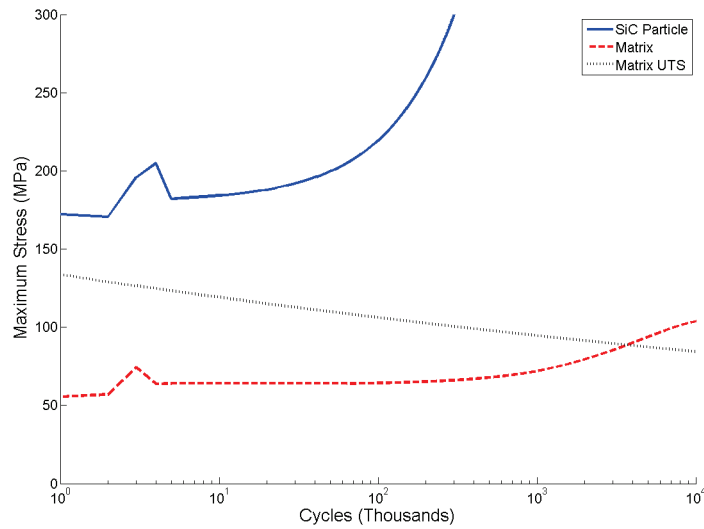


*Figure 4.6: Maximum stress in matrix and SiC particles and matrix UTS based on calculated particle volume fraction for fatigue testing at 240°C with a maximum stress of 100MPa. Failure is predicted to occur at 4.6 million cycles.*

The spikes observed in both particle and matrix stress seen at approximately 3,000 cycles is likely an artifact of the modeling procedure and is unlikely to be an accurate representation of the stress actually experienced by the material. The spike is likely a result of interaction between calculated work hardening and the recovery term. The increase in particle stress is a result of matrix yielding, while the sudden drop occurs due to a large recovery of strain.



## **5. Future work**

### **5.1 Fiber-matrix interface**

Determination of what exactly is occurring at the fiber-matrix interface in both Enfil and Saffil MMCs will help to explain why the interface between Enfil and the A356 matrix appears to be weaker than between Saffil and A356.

### **5.2 Fiber alignment**

Testing of samples with fibers aligned in the loading direction will give a more realistic representation of the loading conditions observed in the brake drum. It is also likely to highlight any differences in fiber-matrix interface strength. Fibers aligned in the loading direction will allow the interface between fiber and matrix to transfer more of the load to the fibers. Fiber alignment is also likely to highlight differences in fiber-matrix interface strength. A weak interface, like what appears to exist in the Enfil MMC, might not allow for complete loading of the fiber before the interface fails.

### **5.3 Interaction between creep and fatigue**

Developing a better understanding of the interaction between creep and fatigue in both composites tested will help more completely understand the failure of the materials. The observed failure mode was not a completely fatigue or completely creep mechanism. No signs of classic fatigue crack initiation and growth were observed on fatigue fracture surfaces. While creep and fatigue failure surfaces were similar in appearance, fewer SiC particles were observed to have failed in creep tests at the same mean stress.

## **6. Conclusions**

### **6.1 Hypothesis**

#### **6.1.1 Shot particle content**

In this work, it was hypothesized that the reduced shot content of Saffil fiber compared to Enfil fiber would result in higher cycles to failure in fatigue. Fewer shot particles will give fewer “defects” in the material that cracks are able to initiate and grow from.

While it was found that Saffil MMCs had higher cycles to failure than Enfil MMCs, the difference did not appear to be a result of the presence of shot particles. Enfil fiber had a significantly higher amount of fibrous material on the fracture surface than Saffil (Figure 3.17). Few of the observed shot particles or fibers in either MMC were broken, but they had de-bonded from the matrix. This suggests that the difference observed in fatigue behavior is more dependent on composition of the fiber rather than the presence of shot particles. The bond between Enfil fibers and the matrix is weaker than that of Saffil fibers and the matrix, making it easier for Enfil fibers to be separated from the matrix.

This difference is likely to become more pronounced if the fibers are aligned in the direction of loading, unlike the transversely aligned fibers in this study. Load is transferred from the matrix to the fibers by shear along the fiber length. The interface between fiber and matrix is responsible for the load transfer. A weak interface will not be able to efficiently load fibers.

#### **6.1.2 Failure Mode**

It was hypothesized that final failure of the composite in high temperature, low cycle fatigue will occur due to matrix overloading once a critical number of SiC particles have fractured. Examination of the fracture surface showed no evidence that fatigue cracks initiated or grew in the composite structure. Instead, regions of ductile and brittle fracture were observed (Figure 3.11). The ductile regions correspond to final failure in the matrix while brittle fracture corresponds to SiC particles. In tensile tests the relative amounts of the ductile and brittle areas correspond to the bulk volume fraction of each constituent (SiC and A356 matrix).

In fatigue the amount of SiC observed on the fracture surface decreases with the majority of final failure occurring in the matrix. This behavior was explained with progressive failure of SiC particles and continuum approach to

examining the stresses in each phase. As particles fracture they are no longer able to carry load as efficiently putting a greater demand on the matrix. Once enough particles have failed, the stress in the matrix exceeds the UTS of the matrix leading to the mainly ductile failure observed. The last few particles to fracture during matrix failure are seen on the fracture surface.

Experimental observation confirmed that the fraction of particles that had broken increases with increasing number of cycles. Modeling showed that as particles fracture, the matrix sees a higher stress that can become greater than the matrix UTS.

## **6.2 Modeling**

Modeling the fatigue behavior of an MMC based on an approach to predicting the stress-strain behavior of a composite was able to predict cycles to failure at 240°C with a maximum stress of 100MPa reasonably accurately. As SiC particles fracture their ability to carry load is reduced significantly. To carry the same load the stress in the remaining undamaged particles and matrix must increase. Particle fracture had to be experimentally determined (section 3.6) and fed into the model. It showed that the stress in both the matrix and SiC particles increases as the fraction of particles carrying load decreases. The stress in the matrix exceeded the UTS of the matrix after 2.5 million cycles while actual failures were observed at 2.4 and 4.3 million cycles.

The model was modified to calculate particle fracture by accounting for matrix yielding and recovery, composite creep and SiC particle strength distribution. By taking these factors into account, the volume fraction of unbroken particles was accurately predicted. The accurate prediction of particle fracture lead to a predicted failure of the composite at 4.8 million cycles, slightly higher than the observed failure range. However one sample tested at the same conditions did not fail after 11.5 million cycles.

The model to predict failure in fatigue due to particle fracture is limited by the limited understanding of creep in the composite. The creep rate of the composite in fatigue is an order of magnitude lower than that observed in pure creep testing at the same mean stress.

## 7. Works Cited

- Babout, L., Y. Brechet, E. Maire, and R. Fougères. 2004. On the competition between particle fracture and particle decohesion in metal matrix composites. *Acta Materialia*. 52:4517-4525.
- Brosnan, M., and S. Shivkumar. 1995. Elevated Temperature Tensile and Fracture Behavior of A356 Castings. *AFS Transactions*. 727-737.
- Brown, L.M. 1975. Work Hardening Due to Internal Stresses in Composite Materials. *Acta Materialia*. 23:821-830.
- Dieringa, Hajo, Norbort Hort, and Karl Ulrich Kainer. 2004. Magnesium Based MMCs Reinforced with C-Fibers. *Advances in Technology of Materials and Materials Processing*. 136-141.
- Ding, H.Z. 2002. A low Cycle Fatigue Model of a short-fiber reinforced 6061 aluminium alloy metal matrix composite. *Composites Science and Technology*. 62:2189-2199.
- Eshelby, J.D. 1957. The Determination of the Elastic Field of an Ellipsoidal Inclusion, and Related Problems. 376-396.
- Eshelby, J.D. 1959. The Elastic Field Outside an Ellipsoidal Inclusion. 561-569.
- Evans, R.D. 2003. Near-interface microstructure in a SiC/Al composite. *Scripta Materialia*. 59-63.
- Gurland, J., and J. Plateau. 1963. The Mechanism of Ductile Rupture of Metals Containing Inclusions. *Transactions of the ASM*. 56:442-454.
- Hall, Jody N, J. Wayne Jones, and Anil K. Sachdev. 1994. Particle Size, Volume Fraction, and Matrix Strength Effects on Fatigue Behavior and Particle Fracture in 2124 Aluminum-SiCp Composites. *Materials Science and Engineering*. A183:69-80.
- He, Chunlin. 2011. Effect of SiC Particle Size on Microstructure and Tensile Behavior of Aluminum Matrix Composites. *Advanced Materials Research*. 2129-2133.

- He, Chunlin. 2011. Tensile Properties of Aluminum Matrix Composites Reinforced With Submicron SiC Particles. *Advanced Materials Research*. 538-541.
- Herr, Alan E., Sridhar Canumalla, and Robert N. Pangborn. 1995. Thermal Fatigue behavior of squeeze cast, discontinuous alumina-silicate reinforced aluminum alloy (A356) composite. *Materials Science and Engineering A*. 181-191.
- Lesuer, D. 1998. Isothermal Fatigue. *Lawrence Livermore National Laboratory*
- Llorca, J. 1993. Failure micromechanisms in particulate-reinforced metal-matrix composites. *Journal De Physique IV*. 1793-1798.
- Lloyd, D.J. 1994. Particle reinforced aluminium and magnesium matrix composites. *International Materials Reviews*. 1-23.
- Mkaddem, A., and M. El Mansori. 2009. On fatigue crack growth mechanisms of MMC: Reflection on analysis of 'multi surface initiations. *Materials and Design*. 3518-3524.
- Murtland, Kevin, Robert Cox, and Christopher Immer. 2006. Attaching Thermocouples by Peening or Crimping. *Nasa Tech Breifs*. March: 19.
- Nan, C.W., and D.R. Clarke. 1995. The Influence of Particle Size and Particle Fracture on the Elastic/Plastic Deformation of Metal Matrix Composites. *Acta materialia*. 44(9):3801-3811.
- Ochi, Yasuo. 2007. Effects of volume fraction of alumina short fibers on high cycle fatigue properties of Al and Mg alloy composites. *Materials Science and Engineering A*. 230-236.
- Rafiquzzaman, MD. 2008. Effect of Whisker Orientation on Monotonic and Fatigue Strength of Aluminium Cast Alloy Locally Reinforced by SiC Particles and Al<sub>2</sub>O<sub>3</sub> Whiskers Under Monotonic and Cyclic load. *Journal of Solid Mechanics and Materials Engineering* 2. no. 1.
- S.F. Corbin, D.S. Wilkinson. 1993. The Influence of Particle Distribution on the Mechanical Response of a Particulate Metal Matrix Composite. *Acta materialia mater*. 42(4):1311-1318.

- Snead, Lance L., Takashi Nozawa, Yuti Katah, Thak-Sang Byun, Sosuke Kondo and David A. Patti. 2007. Handbook of SiC properties for fuel performance modeling. *Journal of Nuclear Materials*. 329-377.
- Sritharan, T. 2001. A feature of the reaction between Al and SiC particles in an MMC. *Materials Characterization*. 75-77.
- Srivatsan, T.S. 2002. Influence of silicon carbide particulate reinforcement on quasi static and cyclic fatigue fracture behavior of 6061 aluminum alloy composites. *Materials Science and Engineering*. 202-214.
- Srivatsan, T.S. 2002a. The fatigue and final fracture behavior of SiC particle reinforced 7034 aluminum matrix composites. *Composites: Part B*. 391-404.
- Tham, L.M., M. Gupta, and L. Cheng. 2003. Predicting the failure strains of Al/SiC composites with reacted matrix-reinforcement interfaces. *Materials Science and Engineering A*. 369-376.
- Wang, Z., and D.J. Lloyd T. Chen. 1993. Stress Distribution in Particulate-Reinforced Metal Matrix Composites Subjected to External Load. *Metallurgical Transactions A*. 24A:197-207.
- Watt, D. F., X. Q. Xu, and D. J. Lloyd. 1996. Effects of Particle Morphology and Spacing On the Strain Fields in a Plastically Deforming Matrix. *Acta materialia* 44(2):789-799.
- Zong, Y., and B. Derby. 1993. Microstructure and fracture behavior of SiCp/Al-2618 metal matrix composite. *Journal de Physique IV*. 1861-1866.

## **Appendix A: Fatigue results**

This section contains complete results for all fatigue tests performed.



*Table A.1: Fatigue results for all samples tested*

Sample ID	Fiber	Stress (MPa)	Temperature (°C)	Cycles to Failure
28-2	Saffil	140	22	11500000+
28-3	Saffil	140	22	11500000+
64-1	Saffil	140	240	217113
64-2	Saffil	140	240	230000
28-13	Saffil	140	240	272447
28-14	Saffil	120	240	494712
28-15	Saffil	120	240	201982
28-16	Saffil	120	240	47518
28-19	Saffil	100	240	2375753
28-21	Saffil	100	240	11500000+
28-22	Saffil	100	240	4255964
28-23	Saffil	140	413	385
28-26	Saffil	140	413	287
28-28	Saffil	120	413	102
28-31	Saffil	120	413	74
28-35	Saffil	120	413	56
28-41	Saffil	100	413	1943
28-42	Saffil	100	413	1592
28-43	Saffil	100	413	1305
30-1	Enfil	140	22	11500000+
30-9	Enfil	140	240	143607
30-11	Enfil	140	240	77192
30-12	Enfil	140	240	162571
30-13	Enfil	120	240	778928
30-14	Enfil	120	240	447806
30-15	Enfil	120	240	846270
30-17	Enfil	100	240	10500000+
30-19	Enfil	100	240	3328529
30-21	Enfil	140	413	20
30-24	Enfil	140	413	10
30-26	Enfil	140	413	12
30-28	Enfil	120	413	47
30-29	Enfil	120	413	55
30-30	Enfil	120	413	101
30-32	Enfil	100	413	330
30-40	Enfil	100	413	308

## Appendix B: Stress distribution in fatigue samples

The stress in a sample as a function of distance from the center of the hour glass shaped fatigue sample geometry was calculated to determine how far away from the center microstructures should be examined.

Radius of hour glass shaped fatigue sample as function of distance from center (inches)

$$y(x) := 2.624 + 0.5i \cdot \sqrt{2.0 \cdot x - 5.0} \cdot \sqrt{2.0 \cdot x + 5.0}$$

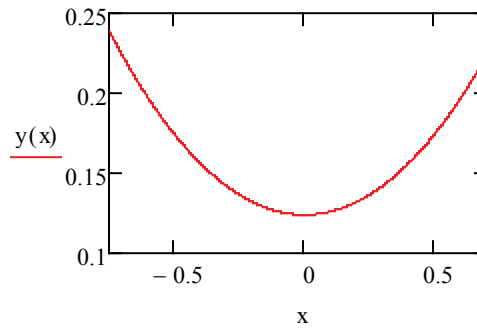


Figure B.1: radius of sample as a function of distance from center

$$\sigma(x) := \frac{\frac{\text{maxload}}{1000}}{\pi \cdot y(x)^2}$$

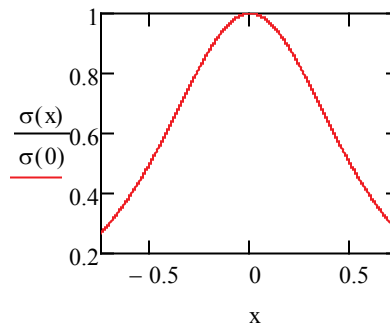


Figure B.2: Stress in sample as a function of distance from center

$$\sigma(.184) = 15.769$$

$$\frac{\sigma(.183)}{\sigma(0)} = 0.9$$

## Appendix C: Tensile Data

The following contains all of the tensile test results from the current study.

*Table C.1*

*Tensile results for all samples tested*

240 °C					
		Elastic Modulus	Yield Strength	Ultimate Tensile Strength	Strain at failure
Sample	Fiber Type	Gpa	Mpa	Mpa	%
30-35	Enfil	122.61	81.94	190.86	1.37%
28-32	Saffil	90.74	86.40	177.78	1.09%
28-30		105.89	103.12	193.37	1.10%
	Average	98.32	94.76	185.58	1.10%
Al-1	A356	27.17	86.18	115.97	19.00%
Room Temperature					
28-20	Saffil	131.51	185.40	270.74	0.52%
30-33	Enfil	145.57	174.51	253.25	0.43%

## Appendix D: Model Code for observed particle fracture

The following is the Matlab code used to calculate the stresses in particles and matrix in the composite based on experimental particle fracture data. This code is executes the procedure outlined in section 4.1

```
%% load data and plot

clc
clf
clear

load stress.txt
load strain.txt
load data.txt
load rtstress.txt
load rtstrain.txt

Em=data(1,1);
yield=data(1,2);
Ep=61931226;
Vpideal=0.4;
Vm=(1-Vpideal);
Ecomp=20e6;

%% fit Ramberg equation to data
guess=[.1,.428,Em,yield];
[newparm]=lsqcurvefit(@Ramberg,guess,stress,strain);

newn=newparm(1);
newa=newparm(2);

stressstep=1;
maxstress=20500;
steps=maxstress/stressstep;
stresss=0:stressstep:maxstress;
mstrain(1)=0;
for i=1:steps
    if stressss(i+1)<=12975
        mstrain(i+1)=((stressss(i)./Em)+(newa).*((stressss(i))./yield).^(1./newn));
    elseif stressss(i+1)>12975;
        mstrain=3.38539e-5*stress-.43502972;
    end
end
fprintf('n= %6.6f \n',newn)
fprintf('a= %6.6f \n',newa)

%% define initial values of stress and strain

stresscomp(1) = 0;
stressp(1) = 0;
stressm(1) = 0;
straincomp(1) = 0;
```

```

strainp(1) = 0;
strainm(1) = 0;

deltastress=400;
damnandblast=.01; %change stress seen in matrix to caculate instant modulus

%% Tensile Iterations !!!!!!!
cycles=11500000;
step=1000;
steps=cycles/step;
stresspmax=zeros(1,steps);
stressmmax=zeros(1,steps);
Vp_v=zeros(1,steps);
Vpcalc_v=zeros(1,steps);
%Create arrays

R=.38;
highstress=14500;
lowstress=highstress*R;
change=highstress-lowstress;
%Define max and min stresses for fatigue

for q=1:steps
j=1;
i=2;
z=1;
Vp=Vpideal*(1-(.0002*sqrt(q*step)+.3887)^2);
%Calculate Vp based on experimental observation
UTS(q)=18*10^3*.979*((q*step)/(3600*20))^-0.05;

if Vp>0
    Vp=Vp;
elseif Vp<=0
    Vp=0;
end
Vp_v(q)=Vp;

stresscomp=zeros(1,iterations);
stressp=zeros(1,iterations);
stressm=zeros(1,iterations);

straincomp=zeros(1,iterations);
strainp=zeros(1,iterations);
strainm=zeros(1,iterations);

stressp(1)=startstressp(q);
strainp(1)=startstrainp(q);
%Create arrays

compguess = 1.6e7;
%Guess value for composite modulus

TolX=100;
while stresscomp(i-1)<=highstress

```

```

Emins=damnandblast/(matrixstrain(stressm(i-1)+damnandblast,Em,newa,yield,newn)-
matrixstrain(stressm(i-1),Em,newa,yield,newn));

compeq = @(Ec) compmod(Vp,Ep,Emins(1),Ec,Vm);
Ec = fzero(compeq,compguess,TolX);
%calculate composite modulus

deltastressp=((5*Ep)/(2*Ep+3*Ec))*deltastress;
%Change in stress of particle
deltastressm=((5*Em)/(2*Em+3*Ec))*deltastress;
%Change in stress of matrix

deltastraincomp=deltastress/Ec;
%Change in composite strainlsqcurvefit
delatstrainp=deltastressp/Ep;
%Change in particle strain
deltastrainm=deltastressm/Em;
%Change in matrix strain

stresscomp(i)=stresscomp(i-1)+deltastress;
stressp(i)=stressp(i-1)+deltastressp;
stressm(i)=stressm(i-1)+deltastressm;

straincomp(i)=straincomp(i-1)+deltastraincomp;
strainp(i)=strainp(i-1)+delatstrainp;
strainm(i)=strainm(i-1)+deltastrainm;

%Ec_vector(j) = Ec;
%Emins_v(j)=Emins(1);
stressmmax(q)=stressm(i-1);
stresspmax(q)=stressp(i-1);
if Vp==0
    stresspmax(q)=0;
end

j=j+1;
i=i+1;

end

disp((q*step))
end

%% Plot
figure(1)
clf
hold on
plot(stresspmax/1000)
plot(stressmmax/1000,'r')
plot(UTS/1000,'k')

```

## Appendix E: Model code for calculated particle fracture

The following is Matlab code used to calculate particle fracture as outlined in section 4.1.2.

```
%% load matrix and composite data

clc
clf
clear

load stress.txt
load strain.txt
load data.txt
load etstress.txt
load etstrain.txt

Em=data(1,1);
yieldm(1)=12000;
Ep=61931226;
Vpideal=0.4;
Vm=(1-Vpideal);
Ecomp=1.45*10^7;

Ky=8000;
n=.2;

%% define initial values and create arrays

deltastress=500;
damnandblast=.01; %change stress seen in matrix to calculate instant modulus

cycles=11500000;
step=1000;
steps=cycles/step;
stresspmax=zeros(1,steps);
stressmmax=zeros(1,steps);
strainmmax=zeros(1,steps);
strainpmax=zeros(1,steps);
yieldm=zeros(1,steps);

good=zeros(1,steps);
dc=zeros(1,steps);
Vp=zeros(1,steps);

startstrainp=zeros(1,steps);
startstressp=zeros(1,steps);

R=.38;
highstress=14500;
lowstress=highstress*R;
change=highstress-lowstress;
%Define max and min stresses for fatigue cycle
```



```

iterations=round(higheststress/deltastress);
%define number of iterations used in calculation of composite stress-strain

failed=0;

recovery=.01;

d0=35;
delta=.4;
K=1160;
%particle distribution and fracture constants

good(1)=1;
broken=0;
yieldm(1)=8000;
creep=0;

compguess = 1.6e7;

TolX=10;

%% calculate stress-strain curve of composite
for q=1:steps

    stresscomp=zeros(1,iterations);
    stressp=zeros(1,iterations);
    stressm=zeros(1,iterations);

    straincomp=zeros(1,iterations);
    strainp=zeros(1,iterations);
    strainm=zeros(1,iterations);

    stressp(1)=startstressp(q);
    strainp(1)=startstrainp(q);

    UTS(q)=16*10^3*.979*((q*step)/(3600*20))^- .05;

    Vpact(q)=Vpideal*(1-(.0002*sqrt(q*step)+.3887)^2);
    Vp(q)=Vpideal.*good(q);
    if q>1
        if Vp(q)>Vp(q-1)
            Vp(q)=Vp(q-1);
        end
    end

    %Calculate Vp for current cycle

    i=2;
    while stresscomp(i-1)<=higheststress
        fish=(matrixstrainworkhard(stressm(i-1)+damnandblast,Em,yieldm(q),Ky,n)-
matrixstrainworkhard(stressm(i-1),Em,yieldm(q),Ky,n));
        if fish==0
            Emin=0;

```

```

else
    Emin=real(damnandblast/fish);
end
compeq = @(Ec) compmod(Vp(q),Ep,Emin(1),Ec,Vm);
Ec(i) = fzero(compeq,compguess,TolX);
% if Ec<0
%     Ec=10;
% end

%calculate composite modulus

deltastressp=((5*Ep)/(2*Ep+3*Ec(i)))*deltastress;
%Change in stress of particle
deltastressm=((5*Em)/(2*Em+3*Ec(i)))*deltastress;
%Change in stress of matrix

deltastraincomp=deltastress/Ec(i);
%Change in composite strainlsqcurvefit
delatstrainp=deltastressp/Ep;
%Change in particle strain
deltastrainm=deltastressm/Em;
%Change in matrix strain

stresscomp(i)=stresscomp(i-1)+deltastress;
stressp(i)=stressp(i-1)+deltastressp;
stressm(i)=stressm(i-1)+deltastressm;

straincomp(i)=straincomp(i-1)+deltastraincomp;
strainp(i)=strainp(i-1)+delatstrainp;
strainm(i)=strainm(i-1)+deltastrainm;

i=i+1;
end

stressmmax(q)=max(stressm);
stresspmax(q)=max(stressp);
strainmmax(q)=max(strainm);
strainpmax(q)=max(strainp);
%Tabulate max stress/strain values

% figure(1)
% hold on
% subplot(2,5,q)
% hold on
% title(q)
% plot(straincomp,stresscomp);
% plot(straincomp,stressp,'r');
% plot(straincomp,stressm,'g');
%Plot stress-compostie strain curves for each cycle

if stressmmax(q)>yieldm(q)
    yieldm(q+1)=stressmmax(q);
elseif stressmmax(q)<=yieldm(q)
    yieldm(q+1)=yieldm(q);

```

```

elseif stressmmax(q)>UTS(q)
    failed=q*step;
end
% Account for strain hardening if matrix stress is over matrix yield

stressMPa=stresspmax(q)*.00689;
dc(q)=(K/(stressMPa))^2;
% calculate critical particle size
good(q+1)=.9*weibull(dc(q),d0,3);
%find weibull cumulative distribution for critical particle size
if good(q+1)>1
    good(q+1)=1;
end
%does not allow Vp to be above Vpideal

plasticstrainm(q)=(strainmmax(q)-(yieldm(q)/Em))*recovery;
%calculate plastic strain in matrix. Assume perfect bonding to
%particles...strain in particle will be equal to strain in matrix
if plasticstrainm(q)>0
    startstrainp(q+1)=startstrainp(q)+plasticstrainm(q);
    %startstressp(q+1)=startstrainp(q+1)*Ep;
    % particles not allowed to go into compression

end

disp(q*step)
%displays a counter
end

%% Plot
figure(1)
hold on
plot(Vp)
plot(Vpact,'r')

figure(2)
hold on
plot(stresspmax/1000)
plot(stressmmax/1000,'r')
plot(UTS/1000,'g')

```

## Appendix F: Additional Matlab functions

Appendix 6 contains Matlab code for various functions called by code in the the models in Appendix 4 and Appendix .

### Composite Modulus

```
function output = compmod(Vp,Ep,Em,Ec,Vm)
```

```
% Function compmod takes Vp, Ep, Em, and is used to solve iteratively for  
% Ec. The form is: 0 = compmod(Vp,Ep,Em,Ec), and can be used with the  
% "fzero" function.
```

```
output = 3*(Ec^2)+((2-5*Vp)*Ep+(2-5*(Vm))*Em)*Ec-2*Ep*Em;
```

### Weibull size distribution

```
function output=weibull(d,L,k)
```

```
%function weibull gives the fraction of partices below a size, d, given the  
%parameters L and k based on a weibull size distribution
```

```
smaller=1-exp(-(d/L)^k);
```

```
output=smaller;
```

### Work hardening matrix strain

```
function output = matrixstrainworkhard(stress,Em,yield,K,n)
```

```
%function matrixstrainworkhard calculates the strain in in a material given  
%the stress, elastic modulus, and values for K and n
```

```
cat=stress;
```

```
if cat<=yield  
    strain = stress./Em;  
elseif cat>yield  
    strain=exp((log((stress-yield)./K)./n))+yield./Em;  
end  
output=strain;
```

### Ramburg-Osgood matrix strain

```
function out=Ramberg(fitparm,input)
```

```
%Function Ramburg calculates the strain in a material based on the stress,  
%material yield stress, and the fitting parameters; a and n
```

```
n=fitparm(1,1);  
a=fitparm(1,2);  
E=fitparm(1,3);  
yield=fitparm(1,4);  
p=length(input);  
for i=1:p  
    outprm(i) = (input(i)/E)+(a)*(input(i)/yield).^(1./n);  
end  
out=outprm';
```

## Appendix G: Displacement due to plastic strain from yielding

Assume composite has stress strain curve as shown:

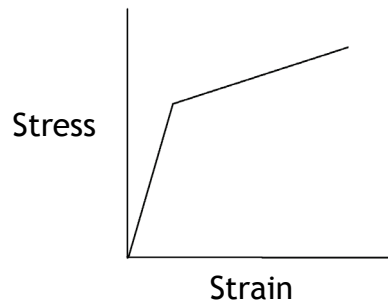


*Figure G.1: Schematic composite stress-strain curve*

$$E(\sigma) := \begin{cases} 12.08 \cdot 10^6 & \text{if } \sigma < 13.74 \\ 2.5 \cdot 10^6 & \text{if } \sigma > 13.74 \end{cases}$$

(modulus values are in english units (msi))

$a$  is the distance from the center of the sample that plastic deformation begins to occur

$$\text{plastic} := \int_{-a}^a \frac{\sigma(x)}{E(\sigma(x))} dx$$

$$\text{plastic} = 1.532 \times 10^{-6} \frac{\text{mm}}{\text{cycle}}$$

# Appendix H: T-test for fatigue tests

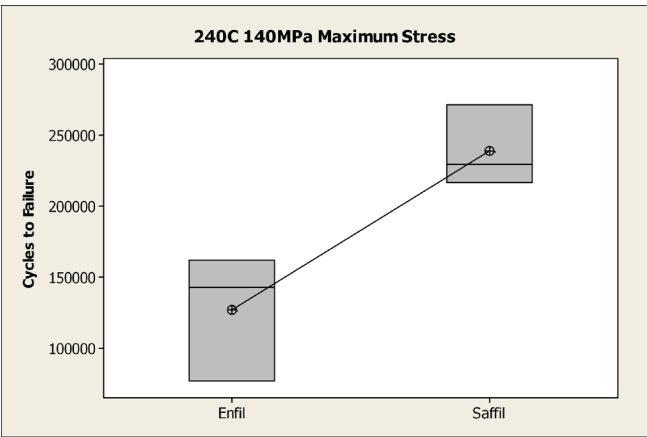


Figure H.1: T-test results for fatigue at 240°C with a maximum stress of 140MPa

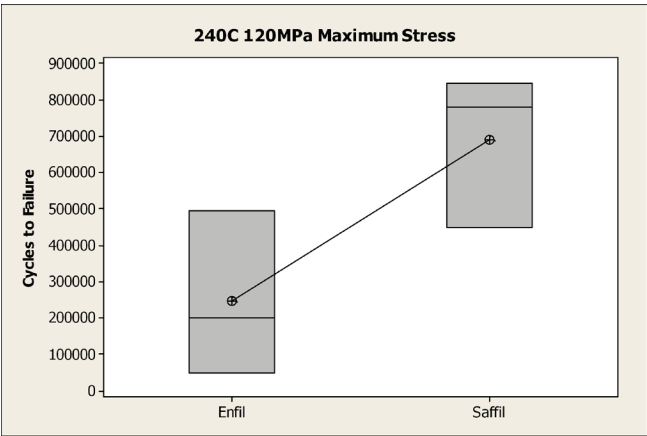
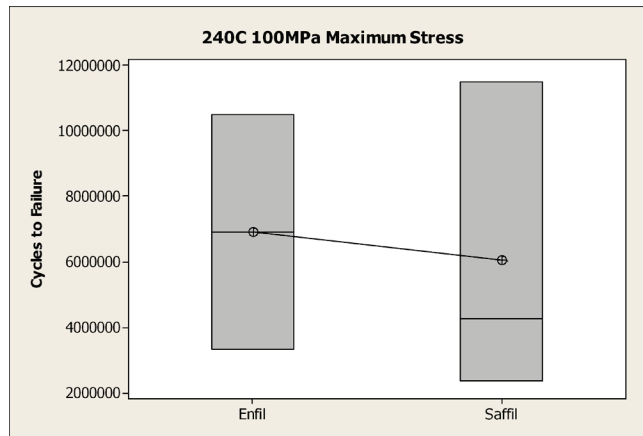
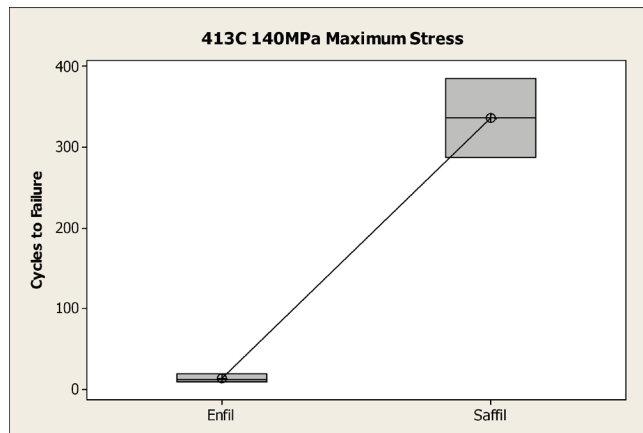


Figure H.2: T-test results for fatigue at 240°C with a maximum stress of 120MPa



*Figure H.3:T-test results for fatigue at 240°C with a maximum stress of 100MPa*



*Figure H.4:T-test results for fatigue at 413°C with a maximum stress of 140MPa*



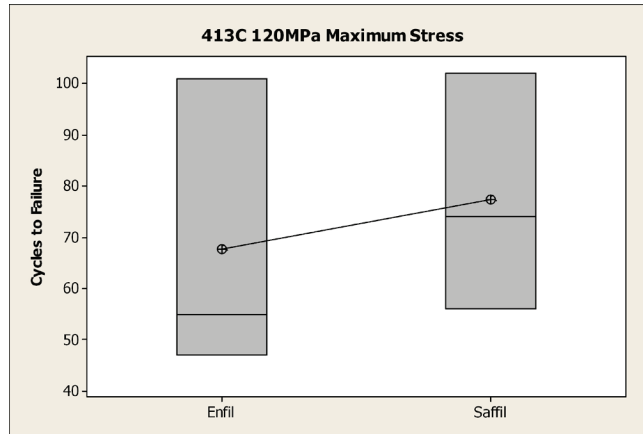


Figure H.5:T-test results for fatigue at 413°C with a maximum stress of 120MPa

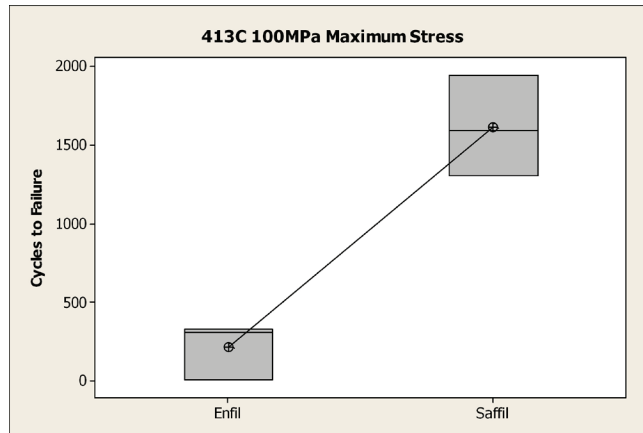


Figure H.6:T-test results for fatigue at 413°C with a maximum stress of 100MPa